Journal of Inflammation Research

Dovepress
Taylor & Francis Group

Open Access Full Text Article

ORIGINAL RESEARCH

Huiyang Shengji Unguent Promotes Lymphangiogenesis and Wound Healing in Diabetic Chronic Wounds: Combined Insights from Proteomics and in vivo and in vitro Analyses

Fangning Yu*, Li Lin*, Xiao Tang*, Xiujuan He, Xuying Xu

Beijing Hospital of Traditional Chinese Medicine, Capital Medical University, Beijing, People's Republic of China

*These authors contributed equally to this work

Correspondence: Xuying Xu, Beijing Hospital of Traditional Chinese Medicine, No. 23, Museum Back Street, Dongcheng District, Beijing, 10010, People's Republic of China, Tel+86- 010-87906642, Email xxying7341@126.com

Purpose: To investigate the mechanism by which HYSJ unguent promotes lymphangiogenesis and improves the healing of diabetic chronic wounds (DCWs).

Methods: The main components of HYSJ were identified by mass spectrometry. A mouse model with chronic skin ulcers was established. The ultrastructure and lymphatic drainage of lymphatic endothelial cells in wounds were examined. Lymphatic markers in wound tissues were detected, and proteomic and bioinformatics analyses were performed to identify differentially expressed proteins and associated pathways. In vitro, a high-glucose inflammatory environment that mimics DCWs was induced in human lymphatic endothelial cells (HLEC). HYSJ and caspase inhibitors were used for intervention. Diverse assays were conducted to assess HLEC function and activation of inflammatory cell death.

Results: The primary constituents of HYSJ unguent included coclaurine, sinapine, and ononin, among others. HYSJ increased healing of DCWs in diabetic mice, protected lymphatic endothelial cells, restored lymphatic drainage in the wound, and upregulated expression of key lymphatic proteins. Numerous proteins, including TLR2, Myd88, STAT1, and inflammatory response-related proteins such as NLRP3, Caspase-1, GSDMD, were expressed differentially in mice. HYSJ unguent also stimulated expression of key lymphatic proteins in HLEC, protected cell function, and suppressed inflammatory cell death.

Conclusion: HYSJ unguent enhances lymphangiogenesis, protects lymphatic endothelial cells in a high-glucose inflammatory environment, and accelerates DCW healing by suppression of TLR2/Myd88/caspase-1 signaling pathway. These findings provide important experimental support for the pharmacological mechanism by which HYSJ unguent facilitates healing of DCWs.

Keywords: traditional Chinese medicine, inflammatory response, TLR2/Myd88 signaling, lymphatic endothelial cells, diabetic wound

Introduction

Diabetes affects over 422 million people worldwide. Impaired wound healing is among the most concerning issues for diabetic patients. For example, almost 10 million patients in China present with diabetic foot ulcers.[1] The annual mortality rate among these patients may be high as 11%, with the amputation rate escalating to 22%.[2] The healing process in diabetic wounds frequently halts in the inflammatory phase during which there is a marked increase in reactive oxygen species and pro-inflammatory cytokines which contribute to compromised cellular function.[3]

Wound healing occurs in a series of distinct and dynamic stages that comprise inflammation followed by granulation tissue formation and subsequent tissue remodeling. Chronic wounds occur when the injury does not progress correctly through these stages which leads to delayed healing or complete failure to heal.[4,5] Current treatment modalities—including debridement, antibiotics, pressure offloading, and conventional dressings—tend to target individual symptoms

Received: 29 May 2025
Accepted: 10 September 2025
Published: 16 September 2025

Graphical Abstract

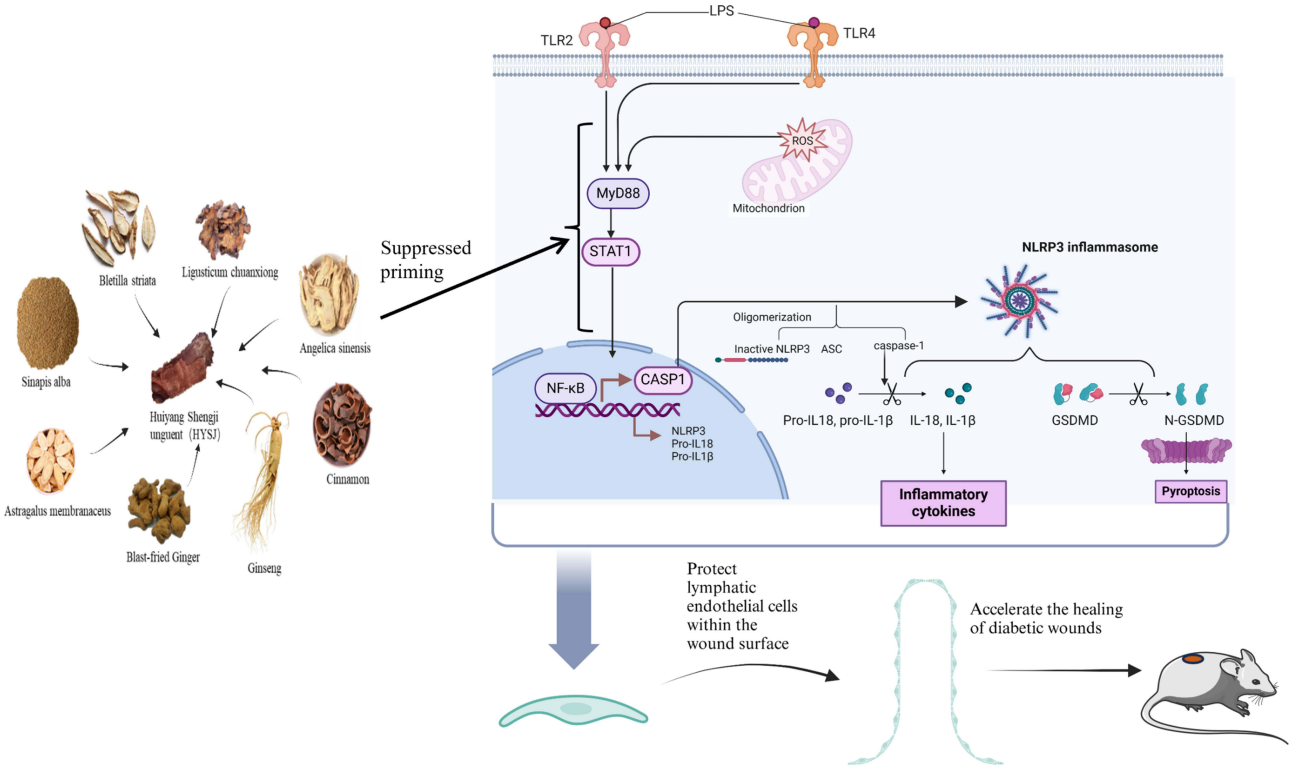

and are often insufficient in promoting complete and sustained healing. Recently, hydrogel-based smart dressings have emerged as promising alternatives to conventional dressings.[6–8] Despite these advances, many such systems rely on synthetic components or novel therapeutic agents with limited translational readiness. Moreover, their role in modulating lymphangiogenesis, a critical but often overlooked process in diabetic wound healing, remains insufficiently studied. The immune regulatory function of the lymphatic system recently has been shown to play a crucial role in chronic inflammatory diseases.[9,10] Expression of the receptor tyrosine kinase vascular endothelial growth factor receptor 3 (VEGFR3) is diminished in human chronic ulcers and pressure sores. This reduction is linked to a decrease in lymphatic vessel density which is connected to altered expression of VEGFR3 in lymphatic endothelial cells (LECs).[11] Moreover, disruption of lymphatic vessel integrity, which often is due to reduced nitric oxide signaling in the wound, typically affects lymphatic function in patients with type 2 diabetes.[12] Dysfunction of the lymphatic system results in sustained and elevated inflammation which is a characteristic feature of chronic wounds. The binding of vascular endothelial growth factor C (VEGF-C) to VEGFR3 is a major driving factor in postnatal lymphangiogenesis.[13] Stimulation of VEGFR3 to promote lymphangiogenesis inhibits chronic inflammation and transgenic VEGF-C delivery alleviates acute skin inflammation.[14,15] Additionally, increased lymphangiogenesis in diabetic wounds alters leukocyte trafficking and extracellular matrix remodeling.[16] Interestingly, the use of an adenoviral vector to overexpress VEGF-C restored lymphatic flow, induced both lymphangiogenesis and angiogenesis, and accelerated wound healing in diabetic mice.[17]

Excessive inflammation is a key mechanism that contributes to the delayed healing of wounds in diabetic patients. This inflammation may be associated with inflammatory necrosis, also known as pyroptosis,[18] which is a newly discovered form of programmed cell death that is activated by inflammasomes. The process eventually leads to membrane rupture. Intracellular components are released as a consequence, which triggers a robust inflammatory response. Growing evidence indicates that inflammasomes induce inflammatory necrosis through a caspase-1-dependent pathway.[19] This process involves diverse cell types, including endothelial cells, vascular smooth muscle cells, and macrophages.[20,21]

Traditional Chinese medicine offers flexible and simple approaches for the treatment of diabetic chronic wounds (DCWs) and Yin-type wounds. These approaches are characterized by multi-target, multi-pathway, and complex regulatory effects that show great potential for therapeutic development. The external drug Huiyang Shengji (HYSJ) unguent has been applied clinically in China for over sixty years with significant efficacy, including for DCWs.[22] Preliminary studies demonstrated that HYSJ unguent regulates the PI3K-AKT pathway, improves oxidative stress in diabetic foot ulcer Yin-type wounds, and promotes fibroblast proliferation.[23] The treatment also stimulates the activity of both endothelial progenitor cells and human umbilical vein endothelial cells.[24] However, the role of HYSJ unguent in regulating lymphangiogenesis in wounds remains unclear.[25] Furthermore, no existing studies have combined proteomics with both in vivo and in vitro analyses to explore the underlying mechanisms of HYSJ in DCW.

This study aims to investigate whether HYSJ unguent promotes lymphangiogenesis in DCWs and explores the molecular mechanisms that are involved. First, we established a DCW mouse model and compared the wound healing rates and the expression of lymphatic endothelial markers in wound tissues following different treatments to determine the relationship between HYSJ unguent administration and lymphangiogenesis. Subsequently, we performed proteomic and bioinformatics analyses on the wound tissues which identified potential pathways and mechanisms involved in the mode of action of HYSJ unguent. These findings were probed further with in vitro experiments to explore the detailed mechanisms by which HYSJ unguent promotes lymphangiogenesis in DCWs. We present evidence that highlights the pivotal role of HYSJ unguent in promoting lymphangiogenesis within DCWs.

Materials and Methods

Preparation of HYSJ Unguent

HYSJ unguent formulation consists of *Panax ginseng* C.A.Mey, *Astragalus membranaceus* (Fisch). Bunge, *Cinnamomum cassia* (L). J. Presl, *Zingiber officinale* Roscoe, *Sinapis alba* L, *Ampelopsis japonica* (Thunb). Makino, *Angelica sinensis* (Oliv). Diels, and *Ligusticum chuanxiong* Hort in a 1:3:1:1:3:1.5:1:1 ratio, and was sourced from the Department of Traditional Chinese Medicine, Beijing Traditional Chinese Medicine Hospital (Beijing, China). Plant nomenclature was verified on March 14, 2025 at http://www.worldfloraonline.org. The herbs were pulverized into a fine powder and passed through a 300-mesh sieve. 100 g of petroleum jelly (Batch No. 110124; Baotou Kunhe Lun Petrochemical Co., Ltd.) was added for every 20 g of herbal powder. The emulsion was mixed thoroughly to form the ointment base which was then applied evenly to gauze strips. Control gauze strips were treated with petroleum jelly only. Based on our previous research[22] and after dose conversion from humans to mice at a 1:9 ratio, the drug concentration in the strips was 0.16 g/cm². Gauze strips underwent high temperature and high pressure sterilization prior to use in animal experiments. The powder was subjected to anhydrous ethanol extraction to maximize the extraction of active components for use in cell experiments.[26] Briefly, 2 g of powder was placed into a 50 mL centrifuge tube and 20 mL of anhydrous ethanol were added. The tube was placed in a beaker containing water and was subjected to ultrasonic extraction for 40 minutes. The supernatant was carefully separated and collected following centrifugation at 3000 rpm for 15 minutes at 4° C. The residual sediment was subjected to a second round of ultrasonic extraction with an additional 20 mL of anhydrous ethanol for 40 minutes. Supernatants from both extractions were combined and evaporated to dryness in a water bath at 60°C to obtain the extract. The desiccated extract was dissolved in complete culture medium, vortexed thoroughly, and sonicated with a vortex mixer and ultrasonic extractor. The solution was subjected to centrifugation at 3000 rpm for 15 minutes at 4°C after which the supernatant was carefully separated and filtered. The filtrate was incorporated into the modeling agent for use in experiments.

LC-MS/MS Component Analysis

HYSJ unguent was added at the required concentrations to a pre-cooled methanol/acetonitrile/water solution (2:2:1, v/v). The mixture was vortexed and subjected to low temperature ultrasonication for 30 minutes, followed by static incubation at −20°C for 10 minutes. The sample was centrifuged at 14,000 *g* at 4°C for 20 minutes, and the supernatant was collected and vacuum-dried. For liquid chromatography tandem mass spectrometry (LC-MS/MS) analysis, the dried sample was reconstituted in 100 µL of an acetonitrile-water solution (1:1, v/v), vortexed, and centrifuged at 14,000 *g* at

4°C for 15 minutes. The supernatant was then injected for analysis in the N Agilent 1290 Infinity LC ultra-high-performance liquid chromatography system (Agilent, California, USA) equipped with an HILIC column for sample separation. Column temperature was maintained at 25°C, with a flow rate of 0.5 mL/min and an injection volume of 2 μL. Mass spectrometric data, including primary and secondary spectra, were acquired using an AB Triple TOF 6600 mass spectrometer (SCIEX, USA). Raw data were processed using XCMS software which performed peak alignment, retention time correction, and extraction of peak areas.

Animals and Grouping

C57BL/6J male mice, aged 8–10 weeks and weighing between 18–23 g, were obtained from Beijing Spebio Biotechnology Co., Ltd. (Beijing, China) (Experimental Animal Certificate No. SCXK - Beijing 2019–0010). Mice were housed in individual cages with free access to food and water. All animal experiments were approved by the Animal Ethics Committee of Beijing Traditional Chinese Medicine Hospital (BJTCM-M-20231202) and conducted in accordance with the Guidelines for the Care and Use of Laboratory Animals and the ethical principles outlined by the Committee on Publication Ethics (COPE). Blood glucose levels were measured by analyzing samples obtained from the tail vein utilizing an Accu-Chek (Berlin, Germany).

After three days of adaptive feeding, 60 mice were fasted for 12 hours without water and body weight was recorded. The mice were divided randomly into control (n=15) and diabetic (n=45) groups according to a random number table Streptozotocin (STZ; 1%) solution was prepared in citrate-citric acid buffer. Mice in the diabetic group were administered daily intraperitoneal injections of STZ (50 mg/kg/day) over a period of five consecutive days to induce diabetes, whereas the control group mice received daily intraperitoneal injections of citrate-citric acid buffer (50 mg/kg/day). The day of the first injection was considered day 0. Blood glucose was measured on days 3, 7, and 14, and mice exhibiting blood glucose levels of 16.7 mmol/L or higher were classified as successful diabetic models. Mice that did not meet this threshold were excluded from the study. Diabetic mice were administered hydrocortisone (20 mg/kg/day; Cat. No. S8050, Solarbio, Beijing, China) by intramuscular injection for three consecutive days after successful modeling.

Mice underwent surgery to create a wound after the final injection. Following intraperitoneal anesthesia with tribromoethanol, a 12-mm full-thickness skin excision was made at the center of the back. Diabetic mice showed a marked rise in both food and water consumption, along with increased urination, following surgery. Additionally, the mice experienced weight loss, displayed dull yellow fur, exhibited white granulation tissue with a thin appearance, and watery exudate at the wound site which confirmed the establishment of a chronic diabetic wound model.[27] Three mice that died postoperatively were excluded from the study.

The remaining 42 diabetic mice were assigned randomly to model (n=15), HYSJ (n=15), and basic fibroblast growth factor (bFGF) (n=12) groups based on a random number table The bFGF group received topical treatment with the growth factor (Cat. No. S20040001, Essexbio, Beijing, China), which was mixed with vaseline to prepare gauze strips. Wound images were captured with a digital camera (Canon, Tokyo, Japan). Skin samples were collected on days 3, 7, and 14 after wound induction. A portion of the wound tissue was preserved in 10% formalin for morphological examination and the remaining tissue was stored at −80°C for subsequent molecular biology analysis.

Protein Profiling and Analysis of Mouse Wound Tissue Post-Administration

Tissue samples were prepared with the iST sample preparation kit (PreOmics, Berlin, Germany). A suitable volume of the sample was combined with 50 μL of lysis buffer, followed by heating at 95°C and 1000 rpm for 10 minutes. After cooling, trypsin digestion buffer was added to the mixture which was then incubated at 37°C with shaking at 500 rpm for 2 hours. The reaction was stopped with termination buffer. Peptide desalting was performed using an iST cartridge and peptides were eluted twice using 100 μL elution buffer. Peptide analysis was conducted using an Ultimate 3000 system (Thermo Fisher Scientific, MA, USA) connected to a reverse-phase column (XBridge C18, 4.6 mm x 250 mm, 5 μm; Waters Corporation, MA, USA) for high pH separation. This separation process was integrated with an EASY-nLC 1200 system and an Orbitrap Lumos mass spectrometer (Thermo Fisher Scientific, MA, USA) to perform low pH nano-HPLC-MS/MS analysis. The acquired raw data were processed and analyzed using Spectronaut X (Biognosys AG, Zurich, Switzerland), with database searches performed with Uniprot. Each sample was prepared by dissolving in 30 μL 0.1%

formic acid in water, and 9 μL of this solution was combined with 1 μL of 10x iRT peptides. The mixture was separated by nano-LC and subjected to analysis using online electrospray tandem mass spectrometry. Data were processed with Pulsar software for database construction.[28] Protein identification was performed by analyzing results with the DDA reference database. Identified proteins were annotated, and differential protein analysis, Gene Ontology (GO) and Kyoto Encyclopedia of Genes and Genomes (KEGG) enrichment analyses, and Gene Set Enrichment Analysis (GSEA) were performed using R software.

Wound Healing Rate

Following capture of wound images, the area of the wound was quantified using Image J software (NIH). The rate of wound healing was determined by Wound Healing Rate (%) = (Initial Wound Area - Post-treatment Wound Area)/Initial Wound Area x100%.

Hematoxylin and Eosin (H&E) Staining

Removed skin tissue was preserved in 4% paraformaldehyde, followed by dehydration, paraffin embedding, and sectioning into 5 μm thick slices. Hematoxylin and eosin staining was performed and morphological changes in the skin were observed by light microscopy. Microscope images were captured using an Axio Imager A2 Zeiss optical microscope (Carl Zeiss, Baden Wurttemberg, Germany).

Transmission Electron Microscope (TEM)

The tissue specimens were fixed with electron microscopy fixative (G1102, Servicebio, Wuhan, China) and 1% osmium tetroxide, dehydrated through a graded ethanol series, and embedded in epoxy resin. Ultrathin sections (60–80 nm) were prepared and stained with uranyl acetate and lead citrate to enhance contrast. Ultrastructural images were then acquired using a transmission electron microscope (HITACHI, Tokyo, Japan).

Western Blot

Wound tissue and cells were lysed with RIPA buffer for protein extraction and total protein concentration was measured with a BCA assay kit (Thermo, Massachusetts, USA). Samples were denatured at 100°C for 10 minutes, an equal volume of sample loading buffer was added, and SDS-PAGE was performed. Proteins were transferred onto a PVDF membrane and incubated with a rapid blocking solution (Cat. No. P3050; New Cell Molecular Biotech Co., Ltd. Suzhou, China) at room temperature for 20 minutes with gentle shaking. The membrane was incubated with the following primary antibodies as required for 10 hours at 4 °C:recombinant anti-NLRP3 antibody (1:1000; Cat. No. 4691S, Abcam, Cambridge, UK), caspase-1 (E9R2D) rabbit mAb (1:1000; Cat. No. 83383; Cell Signaling Technology, Boston, USA), gasdermin D (E9S1X) rabbit mAb (1:500; Cat. No. HA721144; HUAbio, Hangzhou, China), recombinant anti-LYVE1 antibody RM1067 (1:1000; Cat. No. ab314241; Abcam), PROX1 recombinant rabbit monoclonal antibody (1:500; Cat. No.HA722318; HUAbio), Flt-4 rabbit polyclonal antibody (1:1000; Cat. No. ER65750; HUAbio), VEGFC rabbit polyclonal antibody (1:1000; Cat. No. 22601–1; Proteintech, Wuhan, China), STAT1 recombinant rabbit monoclonal antibody (1:1000; Cat. No. ET1612; HUAbio), MyD88 rabbit pAb (1:1000; Cat. No. A0980; Abclonal, Wuhan, China), TLR2 recombinant rabbit monoclonal antibody (1:800; Cat. No. ET1705; HUAbio), or β-actin antibody (1:8000; Cat. No. #52901; Signalway Antibody, Maryland, USA). Goat anti-rabbit IgG(H+L) (HRP) (1:20000; Cat. No. RS0002; Immunoway Texas, USA) subsequently was added and incubated at room temperature for 1 hour. Protein bands were detected with an infrared laser imaging system (LI-COR, Nebraska, USA), and band intensity was quantified using ImageJ software.

Immunofluorescence

Immunofluorescence was performed in accordance with the guidelines specified by the reagent manufacturer (Panovue, Beijing, China). Briefly, tissue sections were dewaxed and cell slides were fixed. Samples were blocked with 5% BSA or goat serum at room temperature for 30 minutes and the blocking solution was discarded. The diluted primary antibody was added and incubated overnight at 4°C. The remaining primary antibody was removed by washing and a fluorescent

secondary antibody specific to the target was applied. Slides were incubated at room temperature for two hours. All subsequent steps were performed in a dark environment. The secondary antibody was retrieved, and slides were washed thoroughly to remove any remaining antibody. Mounting medium supplemented with DAPI was applied. Slides were examined with an LSM800 confocal laser scanning microscope (Carl Zeiss) with images captured using different light source channels. Images were analyzed using ZEN software (v2.3 lite, Carl Zeiss). Three random fields per group were analyzed.

Wound Lymphatic Drainage

Evans blue dye was used to observe lymphatic drainage from wounds on day 14 as described previously.[29] Briefly, 25 μL 4% Evans blue dye (Solarbio) diluted in phosphate-buffered saline (1 μL/gbw) was injected subcutaneously into the mouse wound using a 30 G needle (n=2 per group). Images were captured at five-minute intervals for 30 minutes and were analyzed using ImageJ software.

Quantitative Real-Time PCR (qRT-PCR) for Gene Expression Assay

Total RNA was extracted with RNA reagent, followed by isopropanol precipitation and 75% ethanol wash. RNA was dissolved in RNase-free water and cDNA was synthesized by reverse transcription at 25°C for 5 min, 42°C for 30 min, and 85°C for 5 sec. PCR was performed in 20 μL reactions containing SYBR® Premix Ex Taq™ II, primers, cDNA, and RNase-free water. Each sample was run in triplicate. Reaction mixtures were sealed, briefly centrifuged, and amplified. Primer sequences are listed in Supplementary Table S1. The qPCR program was initiated at 95°C for 30s, followed by 40 cycles of 95°C for 15s and 60°C for 30s, with melting curve analysis from 60°C to 95°C in 0.5°C increments. Relative mRNA expression was determined using the $2^{-\Delta\Delta Ct}$ method, with β-actin serving as the reference gene.

Cells and Grouping

Human lymphatic endothelial cells (HLECs) were provided by Beijing EallBio Biomedical Technology Co., Ltd. (Beijing, China). Cells were cultured in endothelial cell medium (ScienCell, California, USA) containing 5% fetal bovine serum and were maintained in a 37°C incubator with 5% CO_2. HLECs were subcultured upon reaching confluence utilizing 0.125% pancreatin/0.02% EDTA for digestion. Experiments were conducted using 3rd to 9th generation HLECs. A high-glucose (HG) inflammatory environment that simulated DCWs was induced using 25 mM glucose (Sigma, Berlin, Germany) and 40μg/mL lipopolysaccharide (LPS) (Cat. No. L2880; Sigma). Cells were pretreated with 10 nM nigericin (Nig) for 2 hours to induce pyroptosis. Pyroptosis inhibitor AC-YVAD-CMK was purchased from MedChemExpress (Cat. No. HY-16990, New Jersey, USA), dissolved in DMSO, and screened for the appropriate intervention concentration of 30 μM using the Cell Counting Kit-8 (Dojindo, Kumamoto Prefecture, Japan). Ethanol extracts of HYSJ were prepared at low, medium, and high concentrations. The groups were: (1) control (untreated); (2) diabetic model: HG+LPS+Nig; (3) HYSJ low-dose group: HG+LPS+Nig+HYSJ (1.25 mg/mL); (4) HYSJ medium-dose group: HG+LPS+Nig+HYSJ (2.5 mg/mL); (5) HYSJ high-dose group:HG+LPS+Nig+HYSJ (5 mg/mL); 6) AC-YVAD-CMK group: HG+LPS+Nig+AC-YVAD-CMK; and, (7) AC-YVAD-CMK+HYSJ group: HG+LPS +Nig+AC+HYSJ (5 mg/mL). The AC-YVAD-CMK intervention duration was 2 hours. Three replicates were performed for in vitro experiments.

Scratch Assay

Three parallel lines were drawn on the bottom of each well in a 6-well plate, with 0.5 cm spacing between lines. Subsequently, 2×10^5 cells per well were seeded evenly and allowed to adhere for 24 hours until 100% confluence was reached. A 200 μL pipette tip was held vertically to the well bottom and used to make a uniform scratch, ensuring scratches intersected the parallel lines in a cross shape. The spent culture medium was removed, and the wells were rinsed with 1x PBS to eliminate any detached cells and expose the scratch areas. Fresh medium or intervention agents were added to the wells, and the initial position and condition of scratches were recorded by inverted microscopy. The plate was incubated at 37°C, removed after 7 and 21 hours of incubation, and observations and photographs were taken at the appropriate positions under the inverted microscope. The wound healing rate was determined using ImageJ software

to calculate the scratch area. The healing rate was then computed based on the formula: Wound Healing Rate (%) = (Area T_0 - Area T_1) / Area T_0, where T_0 and T_1 are zero hour and either 7 or 21 hours, respectively.

Tube Formation Assay

Matrigel (30 μL) was added to the wells of a 24-well plate and incubated at 4°C overnight to allow for uniform coverage of the plate bottom. The plate was removed and incubated at 37°C for 30 minutes to allow the Matrigel to solidify. Fifty microlitres of cells ($3.5x10^5$/mL) under different intervention conditions were seeded into each well and incubated for 8–12 hours. Tube formation was observed and captured using an inverted live-cell microscope. Total length of tubular structures and the number of tubes in each field were measured and calculated with Image J software.

Lactate Dehydrogenase Assay

Cell culture supernatants were collected, and the lactate dehydrogenase (LDH) release rate was measured using the LDH Cytotoxicity Detection Kit (Cat. No. C0017; Beyotime).

Detection of Pyroptosis

Apoptosis was assessed using the Hoechst 33342/PI dual staining kit (Cat. No. KGA1803-100; KeyGEN BioTECH) according to the manufacturer's instructions, and were analyzed by flow cytometry. Briefly, cells were collected and incubated with Hoechst 33342 at 37°C in a 5% CO_2 incubator for 15 minutes. Any remaining unbound reagents were eliminated by PBS washing. Cells were stained with propidium iodide and incubated in the dark at room temperature for 5 minutes. Flow cytometry analysis was performed using a flow cytometer (Agilent NovoCyte Quanteon, Santa Clara, CA, USA). Necrotic cells were identified as exhibiting double positivity for Hoechst 33342 and PI.

Statistics

Data are presented as the mean ± standard error of the mean (SEM). Statistical significance was assessed using an unpaired *t*-test, while one-way ANOVA with Bonferroni correction for *p*-values was applied for multiple comparisons. Dunnett's test was used for adjustment in instances of unequal variance. Each in vitro experiment was conducted in triplicate. All statistical analyses were performed using GraphPad Prism v8 (GraphPad Software, La Jolla, CA, USA). $P<0.05$ was considered statistically significant.

Results

Identification of the Main Compounds in HYSJ Unguent

The main components of HYSJ unguent were analyzed by LC-MS/MS. Total ion chromatograms in both positive ion and negative ion modes provided a thorough view of sample composition (Figure 1, Table 1 and Table 2). Chromatographic peak measurement data and inferred LC-MS/MS spectra identified the high abundance peaks in HYSJ as coclaurine, sinapine, ononin, calycosin, adenosine, formononetin, niacinamide, sinalbin, [6]-gingerol, and (-)-epigallocatechin.

Blood Glucose Levels and Body Weight in Diabetic Mice

Blood glucose levels and body weight were assessed in the four mice groups (non-diabetic control, diabetic model, bFGF, and HYSJ) (Figure 2A and B). Mice exhibited statistically significant increases in both body weight and blood glucose levels following intraperitoneal administration of STZ to induce diabetes compared to the control, non-diabetic group. No significant differences were observed in body weight or blood glucose levels among the diabetic mouse groups (Figure 2A and B). In addition, the diabetic model group mice exhibited diverse symptoms, including polyphagia, obesity, polydipsia, polyuria, and reduced mobility that were absent from the control group.

HYSJ Unguent Ameliorates the Wound Healing Rate in Diabetic Mice

The rate of wound repair in the diabetic model group was significantly lower ($P<0.05$) compared to the non-diabetic control group at days 3, 7, and 14 after wound induction. In contrast, the wound healing rates in the bFGF, HYSJ and

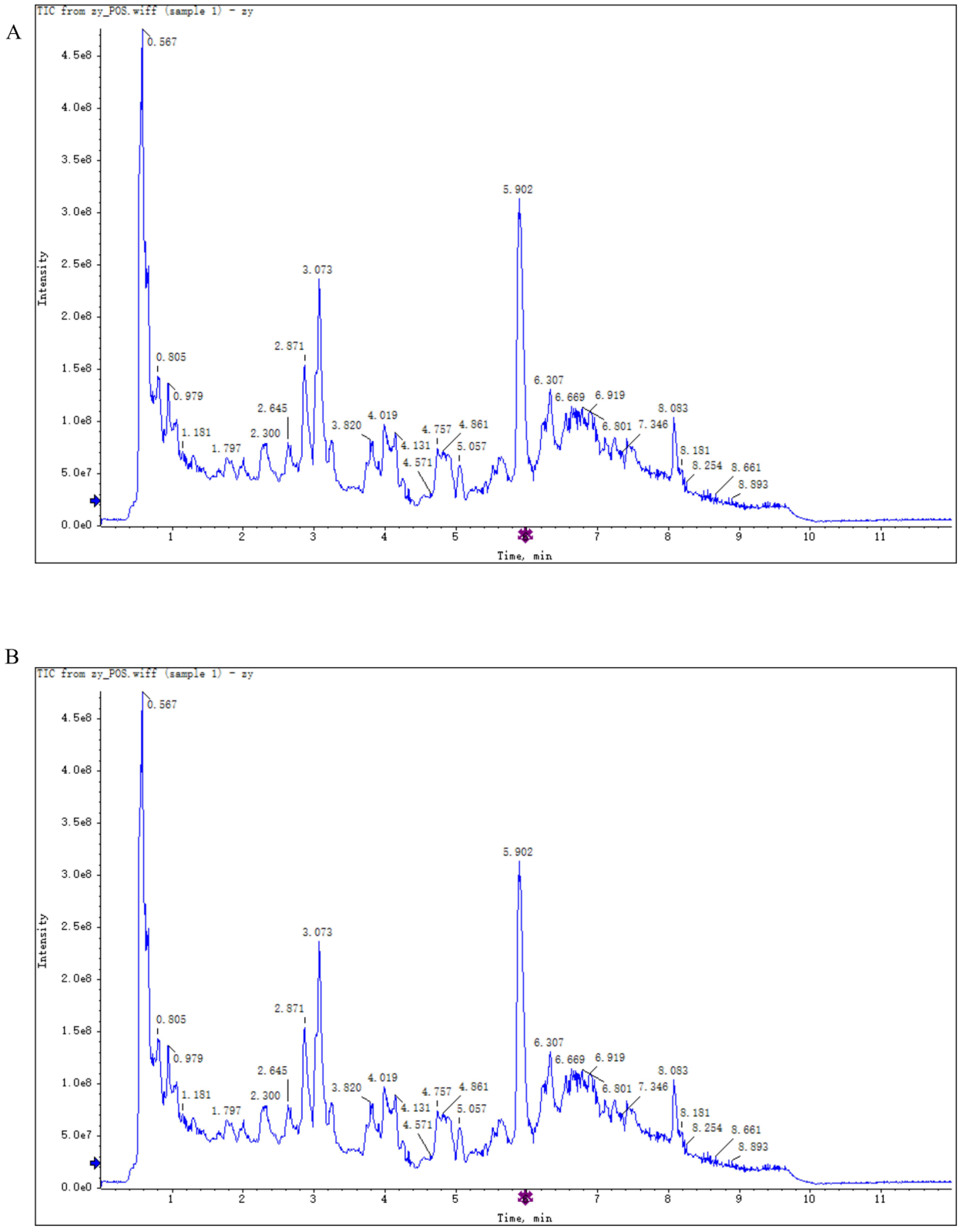

Figure 1 Identification of the components of HYSJ unguent using total ion chromatography in both positive ion (**A**) and negative ion (**B**) modes. The blue arrow is used to mark the retention time.

Table 1 Main Components of HYSJ Unguent in Positive Ion Mode Sorted by Integral Quantitative Value

Index	MS2_Name	RT	m/z	Score	Integral Quantitative Value
M310T173_POS	Sinapine	2.87	310.16	0.99	1.32E+08
M220T231_1_POS	Trans-zeatin	3.84	220.12	0.27	1.1E+08
M365T379_POS	Melibiose	6.31	365.10	0.99	63428994
M104T245_POS	Glycerophosphocholine	4.08	104.10	0.90	54725791
M312T101_POS	Tetrandrine	1.68	312.15	0.18	34009428
M527T434_2_POS	Raffinose	7.23	527.15	0.97	25784284
M381T33_POS	Cytisine	0.55	381.20	0.99	17683031
M431T110_POS	Ononin	1.84	431.13	0.99	16931201
M360T380_POS	Trehalose	6.33	360.15	0.99	16829194
M268T170_POS	Adenosine	2.82	268.10	0.99	16416817
M248T400_POS	Linamarin	6.67	248.11	0.38	14724918
M285T43_POS	Calycosin	0.71	285.07	0.99	13234835
M335T429_POS	Strychnine	7.15	335.15	0.42	6852130
M269T40_POS	Formononetin	0.66	269.08	0.99	5682208
M207T36_POS	Coumarin	0.59	207.06	0.66	5556584
M447T143_POS	Glycitin	2.37	447.12	0.99	5479130
M179T158_POS	Coniferyl aldehyde	2.64	179.07	0.24	5188690
M123T64_POS	Niacinamide	1.07	123.05	0.99	1884346
M370T213_POS	Corydaline	3.54	370.18	0.04	1631443
M286T213_POS	Coclaurine	3.55	286.13	0.89	729577

Table 2 Main Components of HYSJ Unguent in Negative Ion Mode Sorted by Integral Quantitative Value

Index	MS2_Name	RT	m/z	Score	Integral Quantitative Value
M424T183_3_NEG	Sinalbin	3.05	424.04	0.84	1.51E+08
M367T253_2_NEG	Curcumin	4.21	367.10	0.16	18829191
M683T354_NEG	Galactinol	5.90	683.22	0.99	15815509
M279T38_NEG	Linoleic acid	0.62	279.23	0.99	12498827
M191T328_NEG	Quinate	5.46	191.05	0.98	7504766
M128T291_2_NEG	L-pyroglutamic acid	4.84	128.03	0.97	5496679
M401T355_2_NEG	Gentiopicroside	5.91	401.12	0.82	5149831
M293T40_NEG	[6]-gingerol	0.67	293.17	0.33	3443809
M283T43_NEG	Calycosin	0.72	283.06	0.99	2392298
M303T32_2_NEG	N-acetylaspartylglutamic acid	0.53	303.10	0.83	1859111
M408T110_NEG	Glucotropaeolin	1.83	408.04	0.31	1064691
M267T110_NEG	Formononetin	1.83	267.06	0.98	1064433
M217T33_1_NEG	Demethoxycurcumin	0.55	217.05	0.03	1047964
M287T51_NEG	(-)-epigallocatechin	0.85	287.05	0.02	949,135.20
M147T120_2_NEG	Trans-Cinnamate	2.00	147.04	0.97	946,068.30
M122T88_2_NEG	Nicotinate	1.464	122.0244	0.18	879,288.30
M269T33_NEG	Galangin	0.545	269.047	0.12	821,301.60
M337T41_2_NEG	Erucic acid	0.681	337.3105	0.99	701,241.60
M368T173_NEG	Corydaline	2.881	368.1705	0.00	219,525.10

https://doi.org/10.2147/JIR.S534105

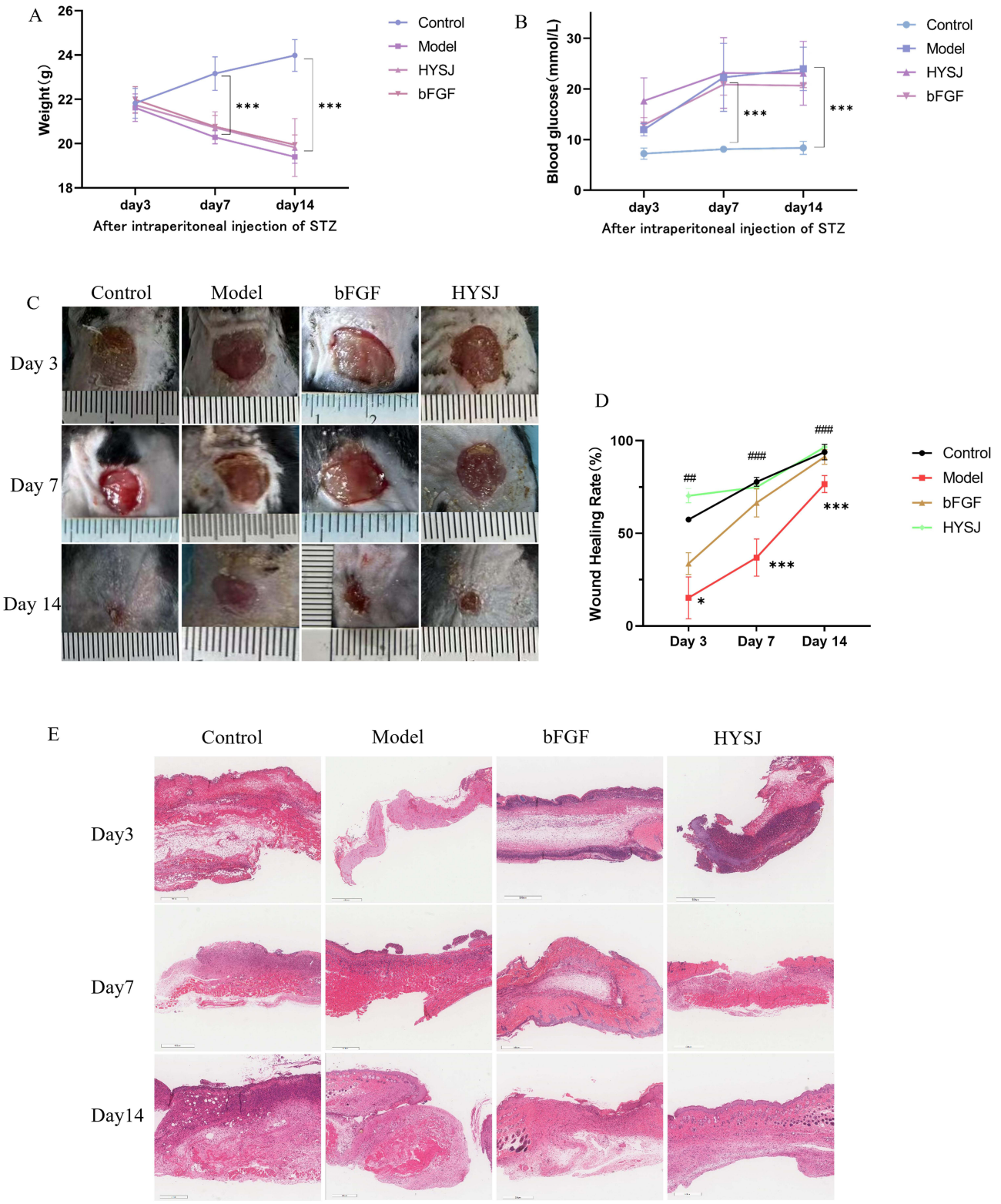

Figure 2 HYSJ unguent accelerates wound closure in diabetic mice with chronic wounds. (**A** and **B**) Variations in body weight and blood glucose of mice at different time points following intraperitoneal injection of STZ (n=5). (**C**) Representative images illustrating wound healing were captured on days 3, 7, and 14 following the surgical procedure. (**D**) Wound closure analyzed using Image J (n=5). (**E**) H&E staining of wound healing tissues on days 3, 7 and 14 after surgery. Scale bar, 500 μm. *P<0.05, ***P<0.001 compared to diabetic model group; ##P<0.01, ###P<0.001 compared to control group.

control groups were substantially higher ($P<0.01$) than in the model group which indicates that HYSJ unguent promotes chronic wound healing in diabetic mice (Figure 2C and D). H&E staining revealed the presence of new epidermal cells in all groups seven days after wound formation. A large number of fibroblasts with uniform arrangement were observed in wounds in the control group. In contrast, the diabetic model group exhibited incomplete epidermal structure, disordered fibroblast arrangement in the dermis, and increased infiltration of inflammatory cells. Diabetic groups treated with either bFGF or HYSJ both exhibited well-preserved epidermal structures that were characterized by tightly packed and orderly arranged fibroblasts, along with a rich network of capillaries. The limited presence of newly formed epidermal cells was evident in both of these groups 14 days after wound induction. In addition, the dermis in the HYSJ group was thicker with more granulation tissue (Figure 2E) which further supports the pharmacological effect of HYSJ unguent in promoting chronic wound healing in diabetic mice.

HYSJ Promotes Lymphatic Endothelial Cells and Lymphatic Drainage in Diabetic Chronic Wounds

Due to the limited ability of HE staining to distinguish lymphatic endothelial cells (LECs) from vascular endothelial cells, we employed TEM to examine the ultrastructural features of LECs in DCWs at 14 days post-intervention (Figure 3A). In the control and HYSJ groups, LECs exhibited a characteristic spindle-shaped morphology with intact oval mitochondria and well-preserved inner and outer membranes. In contrast, LECs in the model group displayed marked morphological abnormalities, including irregular cell shape and organelle disorganization. Notably, mitochondrial swelling and rupture were observed in the model group, accompanied by disruption of both inner and outer mitochondrial membranes. High-magnification analysis further revealed indistinct organelle structures, suggesting significant cellular damage.

We conducted both qualitative and quantitative assessments of lymphatic perfusion in non-diabetic control mice, in diabetic model mice, in diabetic mice treated with bFGF and in diabetic mice treated with HYSJ. Differences between the groups were assessed by examining the lymphatic drainage area which was determined by the spread of Evans blue positivity over a 30-minute period. Both the control and HYSJ animals showed significantly larger dye-positive area at 15 and 30 minutes in comparison with the model group (Figure 3B and C). These results suggest that HYSJ promotes lymphatic drainage in DCWs.

HYSJ Stimulates Expression of Lymphatic Markers in Diabetic Chronic Wounds

Western blot analysis was performed to assess the levels of LYVE-1, PROX-1, VEGFR-3, and VEGF-C in wound tissues of mice at days 3, 7, and 14 post-intervention to determine whether HYSJ promotes the expression of lymphatic protein markers in DCWs. Additionally, we performed co-localization staining for LYVE-1, PROX-1, and VEGF-3 in wound tissue sections on day 14. The expression of LYVE-1 in the HYSJ group increased notably compared to the diabetic model group on day 3 (Figure 4A–E). Moreover, levels of LYVE-1, VEGF-C, and PROX-1 were considerably higher in both the HYSJ and non-diabetic control groups than in the model group on day 7 (Figure 4F–J). Expression of LYVE-1 in the HYSJ group and expression of VEGFR-3, PROX-1, and VEGF-C in both HYSJ and control groups also were significantly higher than those in the model group on day 14 (Figure 4K–O). Fluorescence intensity analysis of lymphatic markers in the tissue at wound sites on day 14 revealed that LYVE-1 expression in the HYSJ, control, and bFGF groups was elevated compared to the model group. Furthermore, expression of PROX-1 and VEGFR-3 increased in both the HYSJ and control groups compared to the diabetic model group at this timepoint (Figure 5A and B) which indicates that HYSJ promotes the expression of lymphatic markers in DCWs.

Proteomic Analysis Reveals Altered Expression of Inflammation-Related and Lymphangiogenesis-Related Proteins Following HYSJ Treatment

The mechanisms by which HYSJ promotes lymphangiogenesis in DCWs were explored by proteomic analysis of wound tissues from non-diabetic control, diabetic model, and HYSJ mice after 14 days of intervention. Bioinformatics analysis was performed using R software to identify differential proteins and pathways which revealed 478 differentially

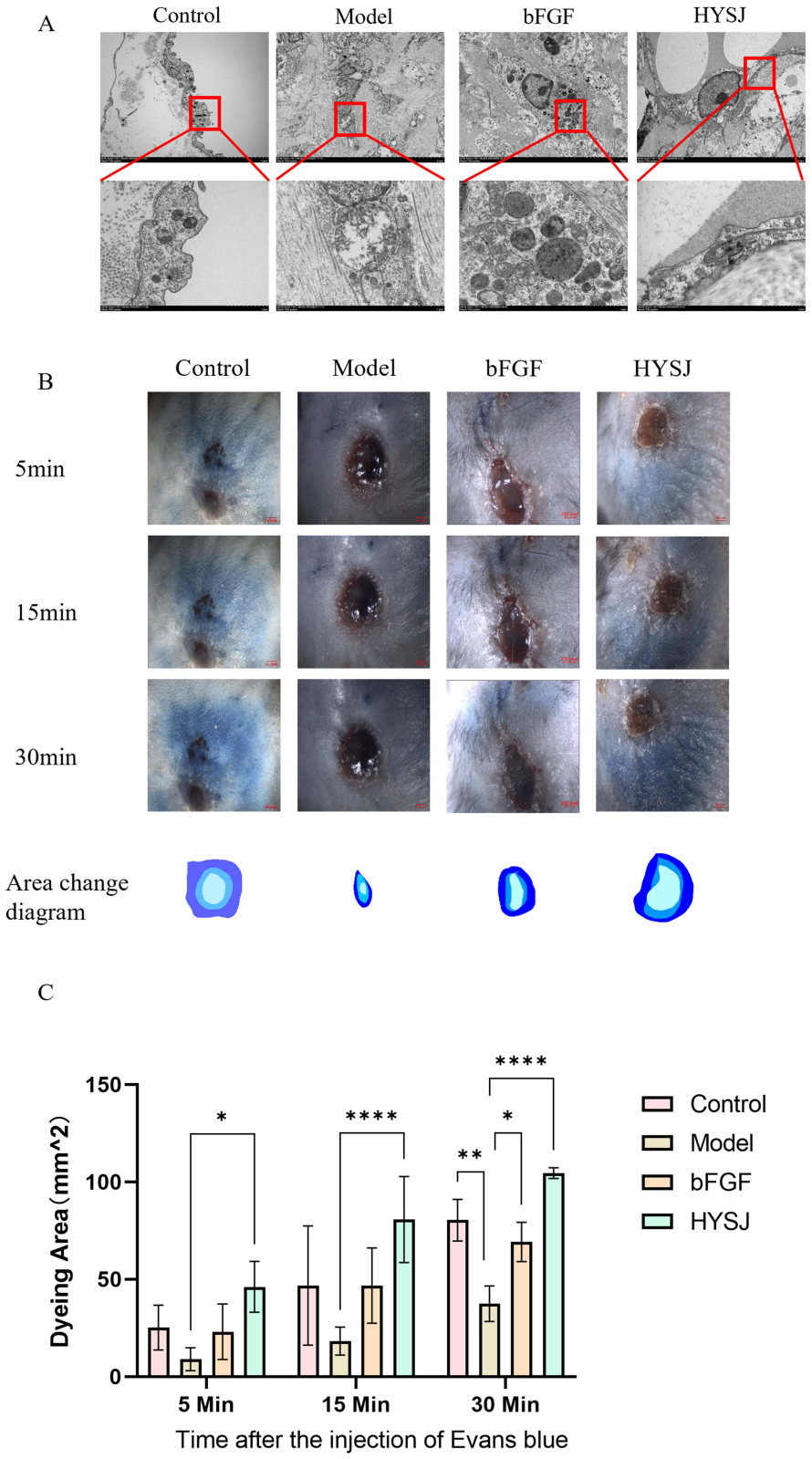

Figure 3 HYSJ protects lymphatic endothelial cells and promotes lymphatic drainage in DCWs. (**A**) Ultrastructural morphology of lymphatic endothelial cells and their organelles at the wound surface under different intervention conditions observed by transmission electron microscope. (**B**) Gross observation results of Evans blue staining positivity on day 14, along with the positive digital contours. The diffusion speed of Evans blue dye was significantly faster in the HYSJ and control groups (n=3 per group). (**C**) Evans blue positivity area. Both the control and HYSJ groups exhibited a higher dye-positive area compared to the model group 15 and 30 minutes after injection. Numbers represent the average value of n=3 for each group. Scale bar, 2 mm. *P<0.05, **P<0.01, ****P<0.0001 compared to model.

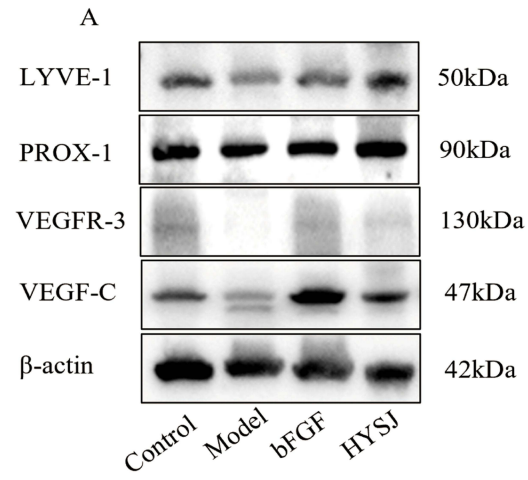

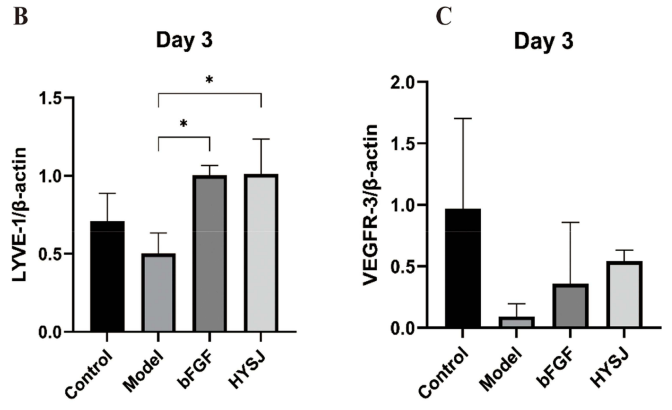

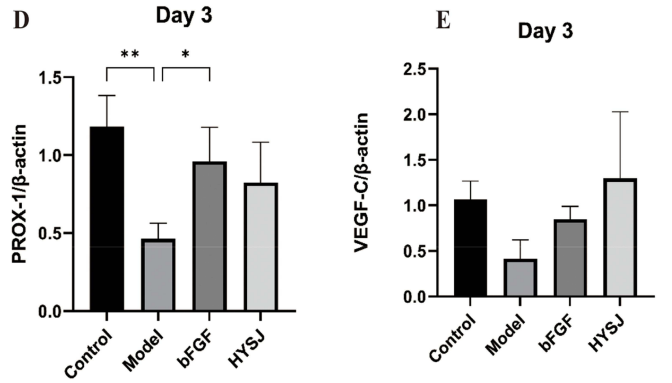

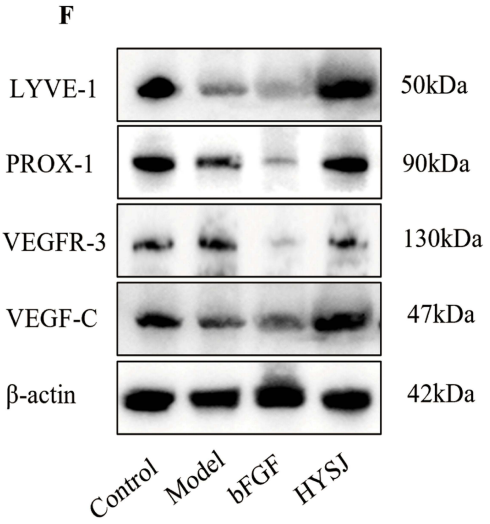

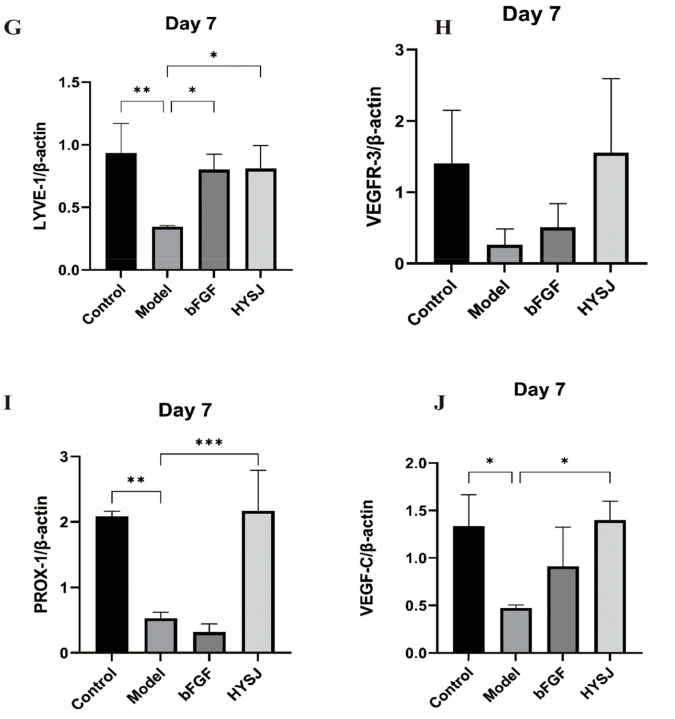

Figure 4 Continued.

https://doi.org/10.2147/JIR.S534105

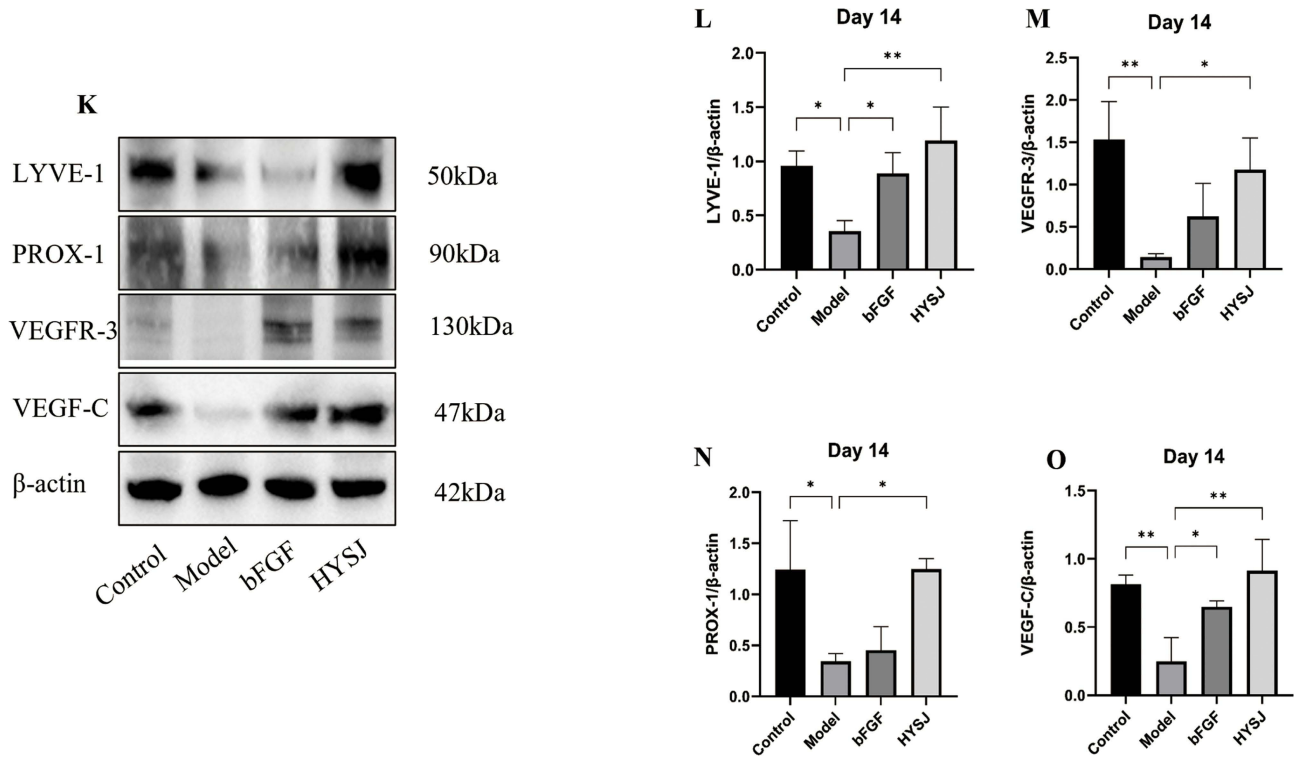

Figure 4 Western blot analysis of lymphatic marker proteins in wound tissues at different time points. (**A**–**E**) Analysis of the relative expression levels of lymphatic markers LYVE-1, PROX-1, VEGFR-3, and VEGF-C, in wound tissues three days after the intervention. (**F**–**J**) Analysis of the relative expression levels of LYVE-1, PROX-1, VEGFR-3, and VEGF-C in wound tissues seven days after the intervention. (**K**–**O**) Relative expression levels and analysis of LYVE-1, VEGFR-3, PROX-1, and VEGF-C in wound tissues on day 14 post-intervention. n=3 per group; *P<0.05, **P<0.01, ***P<0.001.

expressed proteins between control and model groups, 364 differential proteins between control and HYSJ groups, and 311 differential proteins between HYSJ and model groups (Figure 6A). The lymphangiogenesis-related protein FLT4 (VEGFR-3) was downregulated in animals in the model group but was upregulated in control and HYSJ mice. Additionally, pyroptosis-associated proteins gasdermin D and caspase-1 were elevated in the model group, whereas expression was reduced in both control and HYSJ animals (Figure 6B). GO, KEGG, and GSEA enrichment analyses of the differential proteins revealed significant enrichment in the NOD-like receptor signaling pathway which is associated with pyroptosis (Figure 6C and E–G). The Myd88, Stat1, and Tlr2 proteins showed strong interactions with lymphangiogenesis-related protein FLT4 in the protein-protein interaction network (Figure 6D).

Synergistic Effects of HYSJ and Pyroptosis Inhibition on Cell Migration and Tube Formation Function in High Glucose Inflammatory Models

The protective effects of HYSJ on lymphatic vessels in DCWs and examination of the key proteins identified from the preceding omics analysis were probed further with a series of in vitro experiments. The CCK8 method was used to determine the maximum effective concentration of HYSJ intervention in HLECs. A high glucose with LPS and nigericin-induced inflammatory HLEC model was used to simulate the high glucose inflammatory condition in DCWs.

The effects of HYSJ and the pyroptosis pathway inhibitor Ac-YVAD-cmk on HLEC migration were assessed by the scratch assay which revealed that the wound healing area in the HYSJ+Ac-YVAD-cmk group was larger compared to the model group seven hours after the scratch (Figure 7A). In addition, wound healing areas in the control, HYSJ, and HYSJ + Ac-YVAD-cmk groups were greater than in the model group 21 hours post-scratch (Figure 7B) which suggests that HYSJ protects HLEC migration under high glucose inflammatory conditions.

Assessment of the tube formation capacity of HLECs following various treatments (Figure 8A) revealed that both the total branching length and the number of nodes in the control, Ac-YVAD-cmk, and HYSJ+Ac-YVAD-cmk groups were

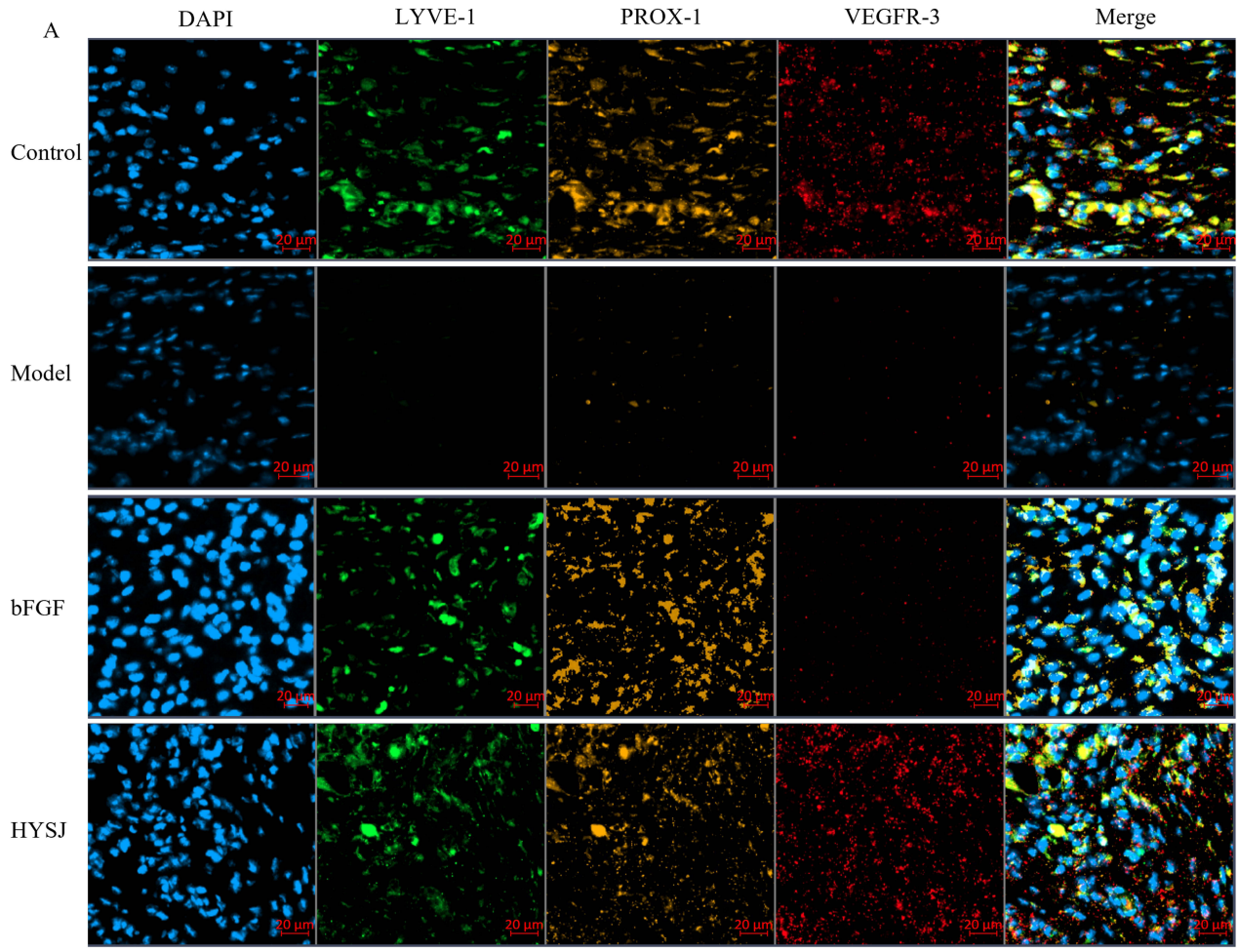

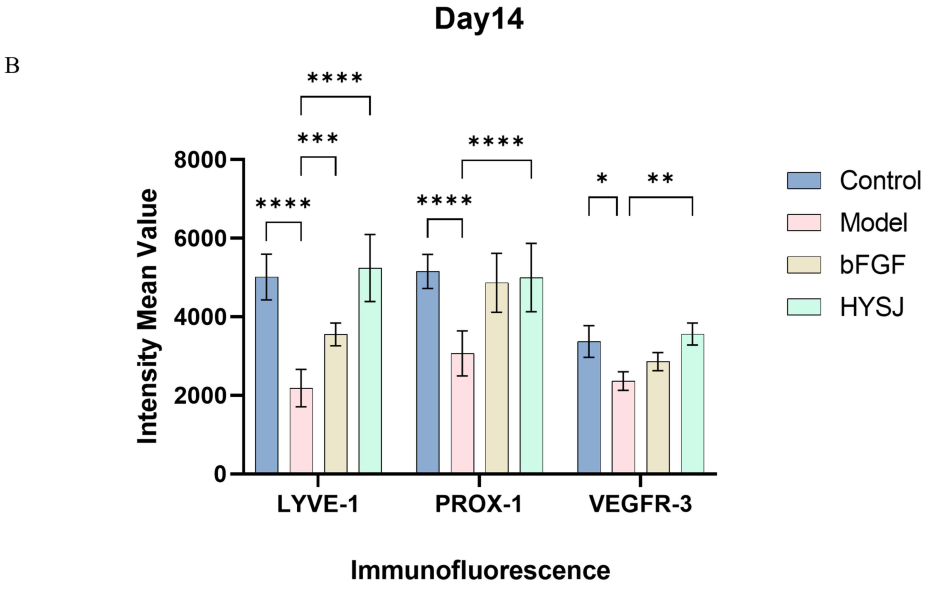

Figure 5 Immunofluorescence triple staining for lymphatic marker expression in wound tissues of mice on day 14. (**A**) Immunofluorescence staining of LYVE-1, PROX-1, and VEGFR3 in wound tissues of mice on day 14. (**B**) Quantitative analysis of fluorescence intensity of lymphatic markers in wound tissues (n=3). Scale bar, 20 μm. *P<0.05, **P<0.01, ***P<0.001, ****P<0.0001.

https://doi.org/10.2147/JIR.S534105

greater compared to model group 12 hours after incubation with Matrigel (Figure 8B and C). Although no significant difference was observed between the HYSJ dose and model groups, the combined treatment with Ac-YVAD-cmk was different from the model group which indicates a potential synergistic effect between HYSJ and the pyroptosis inhibitor Ac-YVAD-cmk. Therefore, we infer that HYSJ may protect tube formation function under high glucose inflammatory conditions by inhibiting the pyroptosis pathway in HLECs.

HYSJ and Ac-YVAD-Cmk Modulate Levels of Key Lymphatic Marker Proteins in HLECs in a High Glucose Inflammation Model

The expression of key lymphatic marker proteins LYVE-1, PROX-1, VEGFR-3, and VEGF-C in HLECs after different interventions was assessed using Western blot analysis (Figure 9A). Expression of LYVE-1 and PROX-1 in the high-dose HYSJ, Ac-YVAD-cmk, Ac-YVAD-cmk+HYSJ, and control groups was considerably higher than in the model group. Moreover, the relative expression of VEGFR-3 in the Ac-YVAD-cmk+HYSJ mice surpassed that observed in the model group, whereas expression of VEGF-C in the high-dose HYSJ, medium-dose HYSJ, Ac-YVAD-cmk, Ac-YVAD-cmk +HYSJ, and control groups was elevated compared to the model group (Figure 9B–E). The relative expression of PROX-1 mRNA was significantly higher in HYSJ group than in model group (Figure 9F).

HYSJ and AC-YVAD-CMK Restrain Production of Inflammatory Cell Death Proteins in HLECs in a High Glucose Inflammation Model

The effects of HYSJ on Inflammatory cell death related pathways in HLECs in the high glucose inflammation model were assessed further by Western blots that detected the expression of TLR2, Stat1, and Myd88 which were identified as

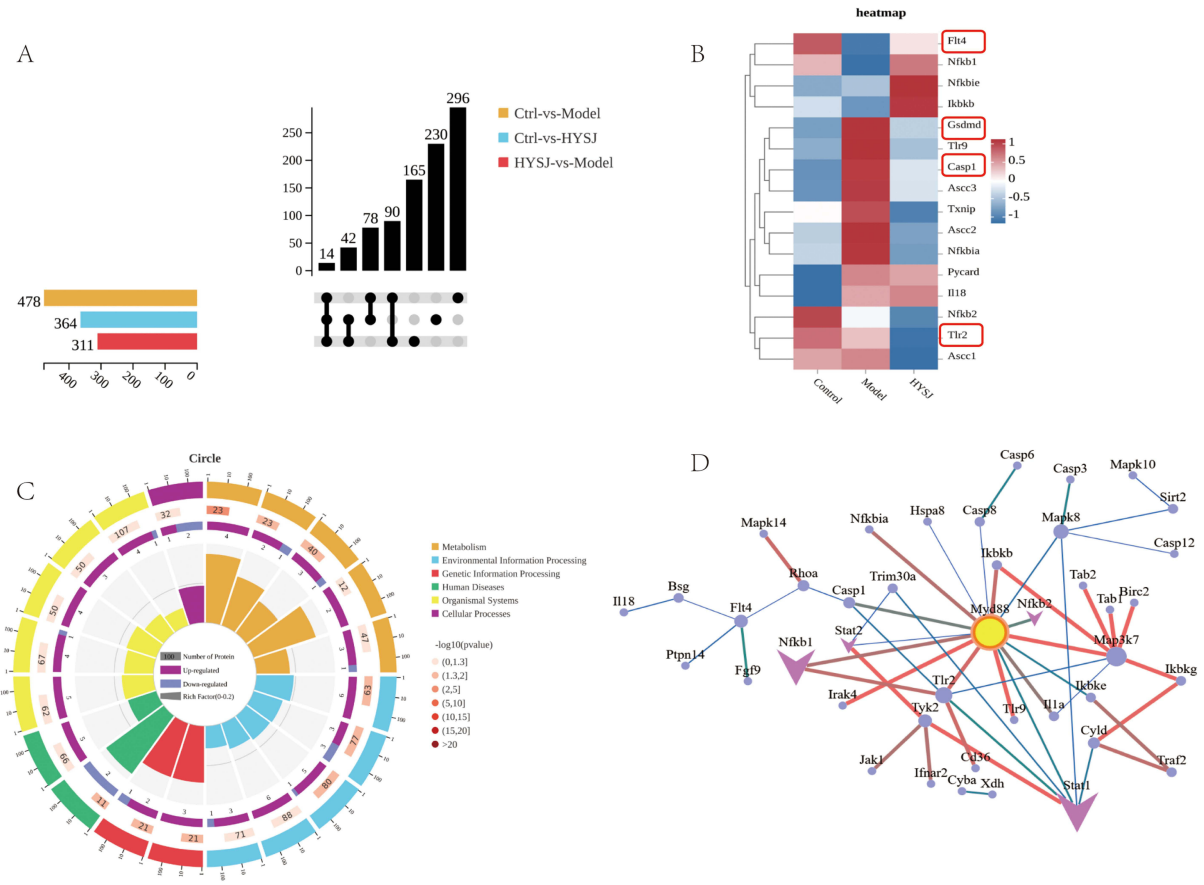

Figure 6 Continued.

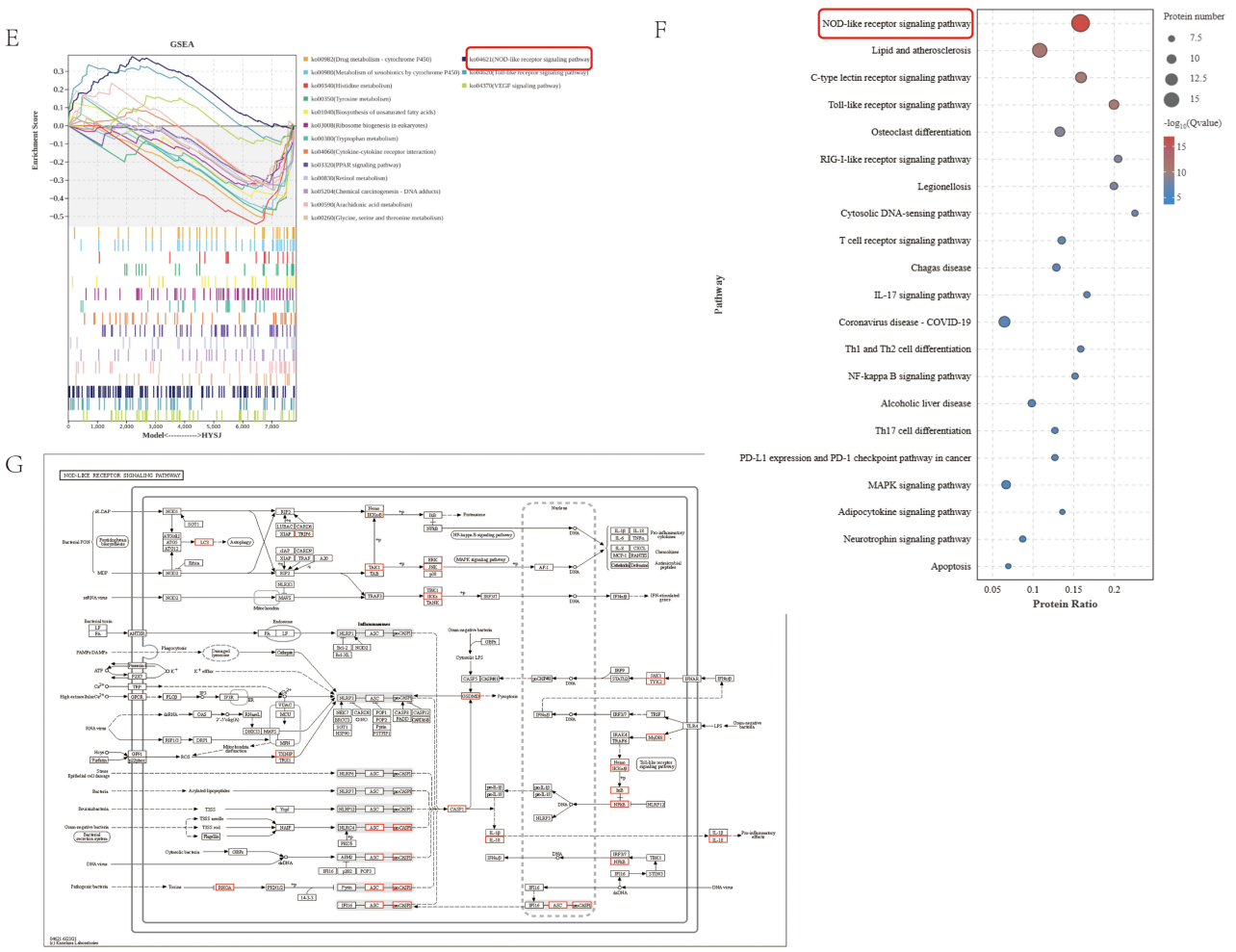

Figure 6 Proteomic analysis of wound tissues in control, HYSJ, and model groups after 14 days of intervention (n=3 per group). (**A**) Upset plot of differential proteins. (**B**) Heatmap of differential proteins. (**C**) Differential GO enrichment analysis plot. The first circle represents the GO term ID with different colors distinguishing different ontologies. The second circle represents the number of proteins in the background that are enriched in the terms; the color indicates the enrichment significance with red indicating higher significance. The third circle illustrates the quantity of differential proteins that are enriched within the respective terms with purple indicating upregulation and blue indicating downregulation. (**D**) Protein-protein interaction network of differential proteins. (**E**) Differential GSEA plot. (**F**) Differential KEGG analysis plot. (**G**) Differential KEGG pathway map. The red boxes represent the pathways and proteins that are the focus of this study.

differential proteins in the proteomics analysis (Figure 10A). The production of inflammation-associated proteins NLRP3, caspase-1, gasdermin D, and N-gasdermin D also was examined by immunoblotting (Figure 10E) and expression of N-gasdermin D additionally was studied by immunofluorescence (Figure 10J). Levels of TLR2 and Myd88 expression in HLECs from all HYSJ treatment groups and in the non-diabetic control group were reduced significantly. Furthermore, Stat1 production in both the high-dose HYSJ and control groups was significantly lower than observed in the diabetic model group (Figure 10B–D). Moreover, the expression of NLRP3/caspase-1/GSDMD pathway proteins in HLECs from all HYSJ dose groups, as well as in the Ac-YVAD-cmk, Ac-YVAD-cmk+HYSJ, and control groups, was reduced markedly compared to the diabetic model group (Figure 10F–K). The extent of Inflammatory death in HLECs after different interventions was assessed further by measuring levels of the LDH tissue damage marker in cell supernatants (Figure 10L). HYSJ effectively lowered LDH levels in a dose-dependent manner in the supernatant of HLECs in the high glucose inflammation model. This effect was enhanced in combination with the pyroptosis inhibitor Ac-YVAD-cmk (Figure 10L). In summary, HYSJ reduces the expression of NLRP3/caspase-1/GSDMD pathway proteins in HLECs in a high glucose inflammation model, and this effect generally is enhanced in the presence of Ac-YVAD-cmk.

https://doi.org/10.2147/JIR.S534105

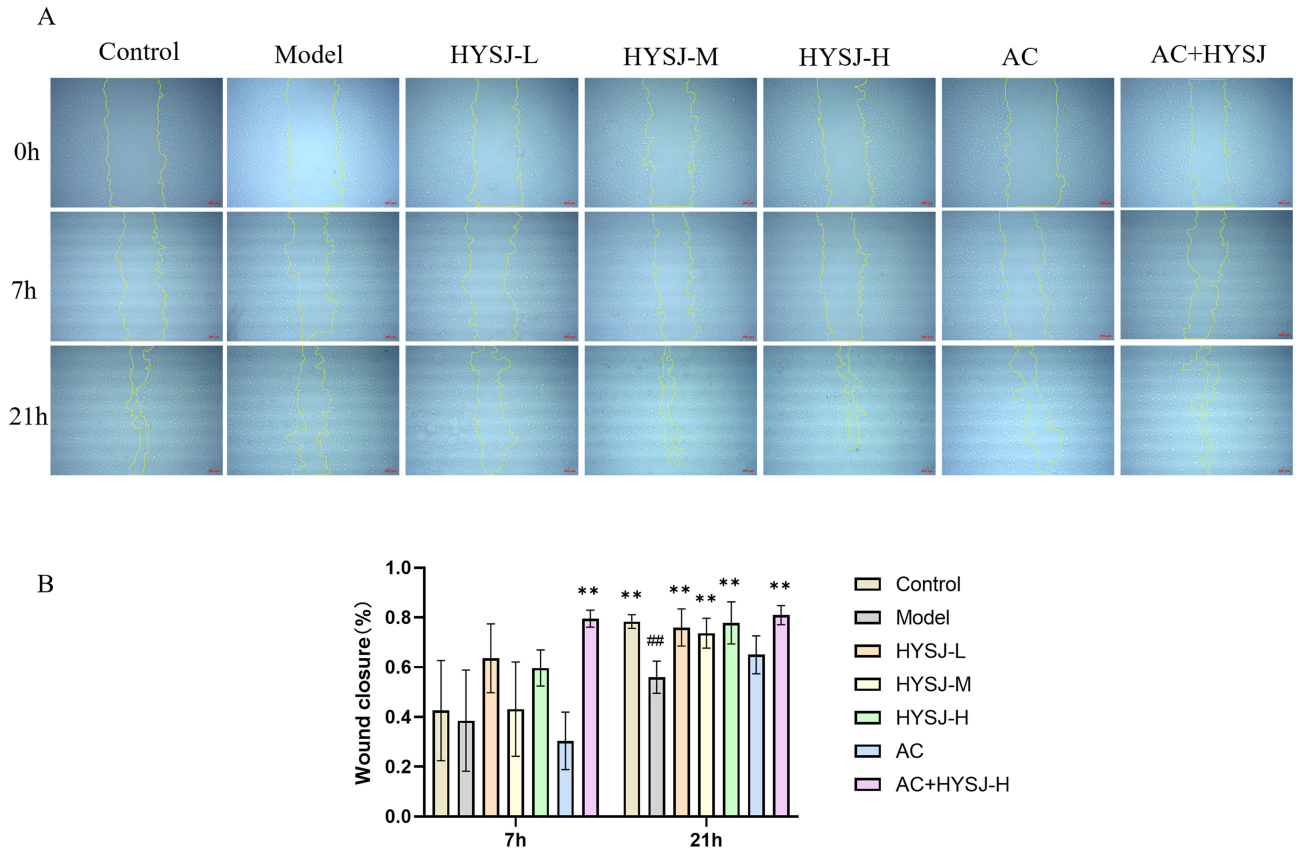

Figure 7 HYSJ improves LEC migration ability. (**A**) Migration images of LECs at 0, 7, and 21 h after the indicated interventions. Scale bar, 200 μm. (**B**) Comparison of wound healing area at different time points. N=3; **P<0.01 compared to model group, ##P<0.01 compared to control group.

Flow Cytometric Detection of Inflammatory Death in HLECs in the High Glucose Inflammation Model After Treatment with HYSJ and Ac-YVAD-Cmk

The Hoechst/PI staining kit was used to distinguish between normal, apoptotic, and inflammatory death cell populations of HLECs following administration of HYSJ or Ac-YVAD-cmk. Samples were analyzed by flow cytometry (Figure 11A–G). The percentage of cells experiencing inflammatory death in both the low and high-dose HYSJ groups was reduced markedly compared to the diabetic model group, and this effect was enhanced by co-treatment with Ac-YVAD-cmk (Figure 11H). These data verify that HYSJ ameliorates inflammatory death in HLECs and that Ac-YVAD-cmk enhances this effect.

Discussion

DCWs are persistent and difficult-to-heal injuries or ulcers that result from diabetes. These wounds not only impact patient quality of life but also may lead to more severe complications, including infection spread, ulcers, and limb amputation. Therefore, early diagnosis and treatment of DCWs are crucial for patient health. Here, we demonstrated that HYSJ unguent promotes the healing of DCWs, enhances lymphangiogenesis in wound tissue, and protects the function of HLECs in a high glucose inflammation model by inhibiting pyroptosis, a pro-inflammatory type of programmed cell death. This effect is associated with the alleviation of chronic inflammation at the wound site and suppression of the TLR2/Myd88/caspase-1 signaling pathway.

In this study, UPLC-MS/MS was employed to identify the major compounds in HYSJ ointment which revealed that the high-abundance peak compounds were coclaurine, sinapine, ononin, calycosin, adenosine, formononetin, niacinamide, sinalbin, [6]-gingerol, and (-)-epigallocatechin. Calycosin has been shown to reduce neuronal pyroptosis and inflammatory injury by targeting the HMGB1-NLRP3-caspase-1 axis,[30] while formononetin modulates NF-κB/NLRP3 signaling in models of asthma and spinal cord inflammation.[31] Ononin attenuates colitis by inhibiting mitochondrial

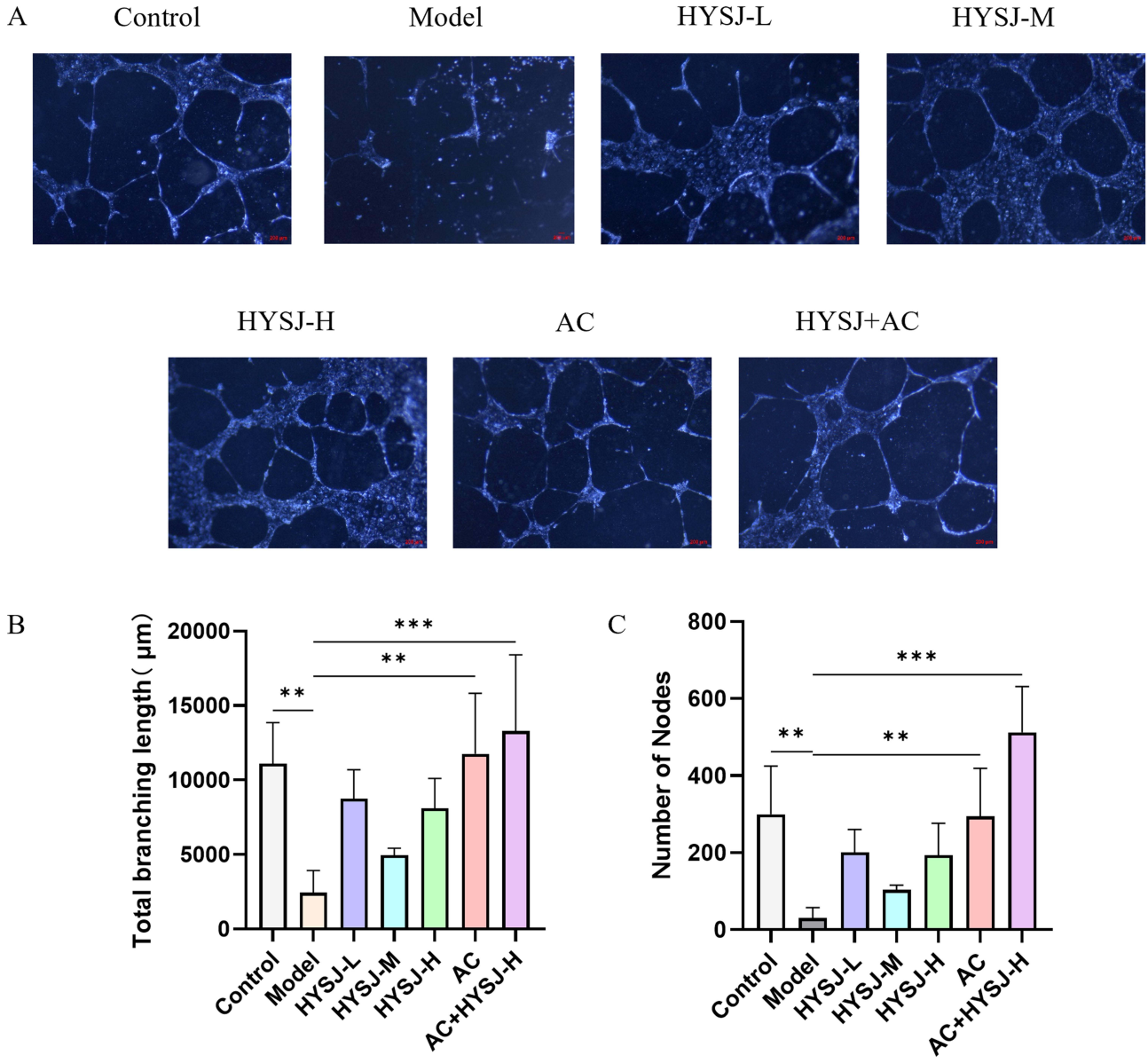

Figure 8 HYSJ protects the tube formation function of HLECs. (**A**) Tube formation images of HLECs in Matrigel after the indicated interventions. (**B**) Analysis of total branching length after the indicated interventions. (**C**) Analysis of the number of nodes after the indicated interventions. N=3; **P<0.01, ***P<0.001 compared to model group. Scale bar, 200 μm.

damage and activating mitophagy to suppress NLRP3.[32] Furthermore, epigallocatechin has demonstrated the ability to modulate VEGF-C expression and enhance lymphangiogenesis in ocular disease models;[33] Adenosine promotes lymphangiogenesis through A2A receptor-mediated VEGFR2 activation, independent of VEGF ligand activity.[34] These findings suggest that the observed therapeutic effects of HYSJ Unguent in diabetic wound healing may be attributed to the synergistic actions of these phytochemicals.

The healing rate of DCWs increased compared to the diabetic model group following intervention with HYSJ unguent and was accompanied by elevated expression of lymphatic marker proteins and an expanded lymphatic drainage area. These findings indicate that one mechanism by which HYSJ unguent promotes wound healing is through the enhancement of lymphangiogenesis. Recent studies have demonstrated that chronic wounds often are accompanied by local lymphatic dysfunction, and the lack or abnormality of lymphangiogenesis may be a key factor that contributes to prolonged non-healing of chronic wounds.[35,36] Lymphangiogenesis promotes healing by facilitating the return of

https://doi.org/10.2147/JIR.S534105

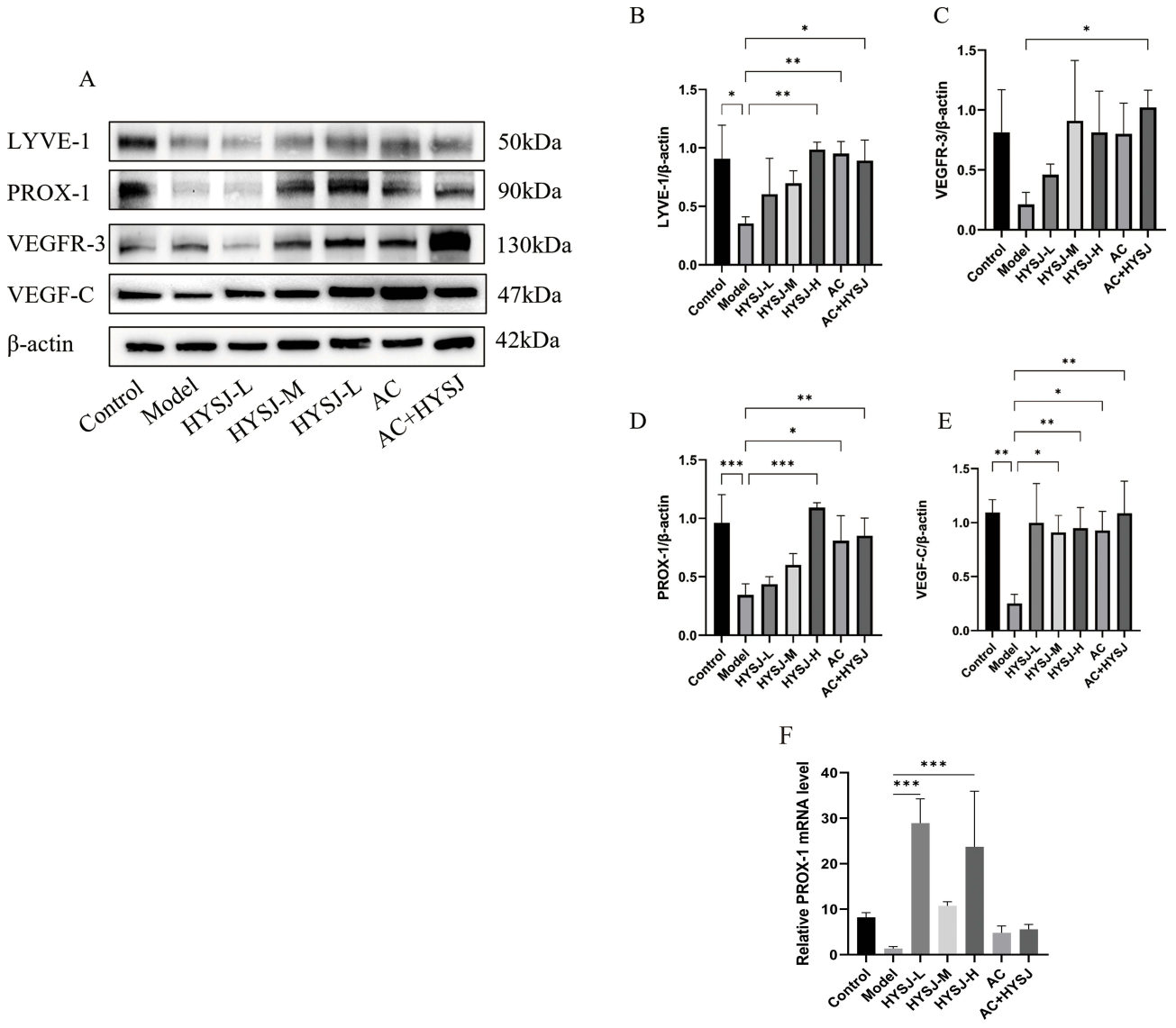

Figure 9 HYSJ promotes the expression of key lymphatic marker proteins in HLECs. (**A**) Western blot detection of key proteins in HLECs. (**B**–**E**) Expression levels of key proteins in HLECs. Each group n=3. * P<0.05, **P<0.01, ***P<0.001 compared to model group. (**F**) Analysis of the relative expression level of prox-1 mRNA.

interstitial fluid, maintaining normal tissue fluid homeostasis, reducing the accumulation of inflammatory cells, regulating the transport of immune cells, and accelerating the clearance of metabolic waste. Impairment of lymphangiogenesis leads to persistent edema and delayed clearance of cellular debris and inflammatory cells.[16] The number and function of lymphatic vessels in ulcerative tissue in diabetic patients are reduced compared to normal tissue which may lead to the accumulation of metabolic waste and inflammatory mediators in the wound, thereby hindering the healing process. Enhanced lymphangiogenesis significantly reduces tissue edema in chronic wound murine models which improves the local microenvironment and promotes wound healing.[37]

bFGF has been reported to exert lymphangiogenic effects. Topical administration bFGF was shown to increase lymphatic vessel density and upregulate VEGF-C in experimental lymphedema models.[38] Additionally, bFGF induced both angiogenesis and lymphangiogenesis in corneal neovascularization models, indicating the shared and overlapping mechanisms in vascular remodeling.[39] Therefore, bFGF served as a biologically relevant positive control to evaluate the efficacy of HYSJU in promoting lymphatic regeneration.

The expression of LYVE- increased markedly on day 3 following administration of HYSJ to wound tissues, and levels of LYVE-1, VEGF-C, and PROX-1 were elevated on days 7 and 14. LYVE-1 is a hyaluronan receptor that belongs

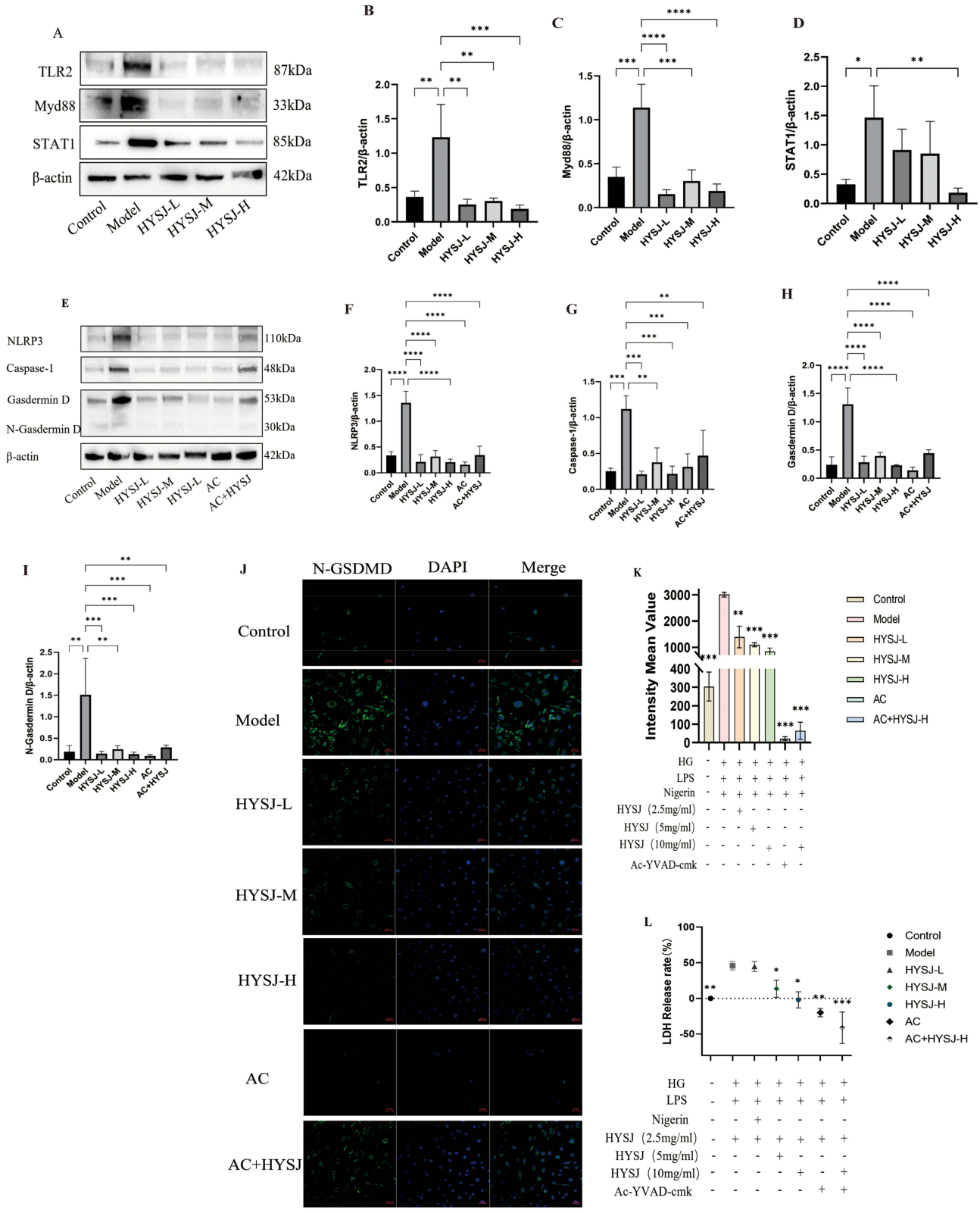

Figure 10 HYSJ inhibits activation of the pyroptosis pathway in HLECs in a high glucose inflammation model. (**A**) Western blot analysis of upstream proteins involved in pyroptosis, including TLR2, Myd88, and Stat1, in HLECs under the indicated conditions. (**B–D**) Relative expression level analysis of TLR2, Myd88, and Stat1 proteins. (**E**) Pyroptosis pathway proteins NLRP3, caspase-1, gasdermin D, and N-gasdermin D expression. (**F–I**) Relative expression of pyroptosis pathway proteins NLRP3, caspase-1, gasdermin D, and Ngasdermin D. (**J**) Immunofluorescence detection of N-gasdermin D expression in HLECs under the indicated intervention conditions. (**K**) Fluorescence intensity analysis of Ngasdermin D in each group. (**L**) LDH levels in supernatants of HLECs under the indicated intervention conditions. Each group n=3. *P < 0.05, **P < 0.01, ***P<0.001, ****P < 0.0001 compared to model group.

https://doi.org/10.2147/JIR.S534105

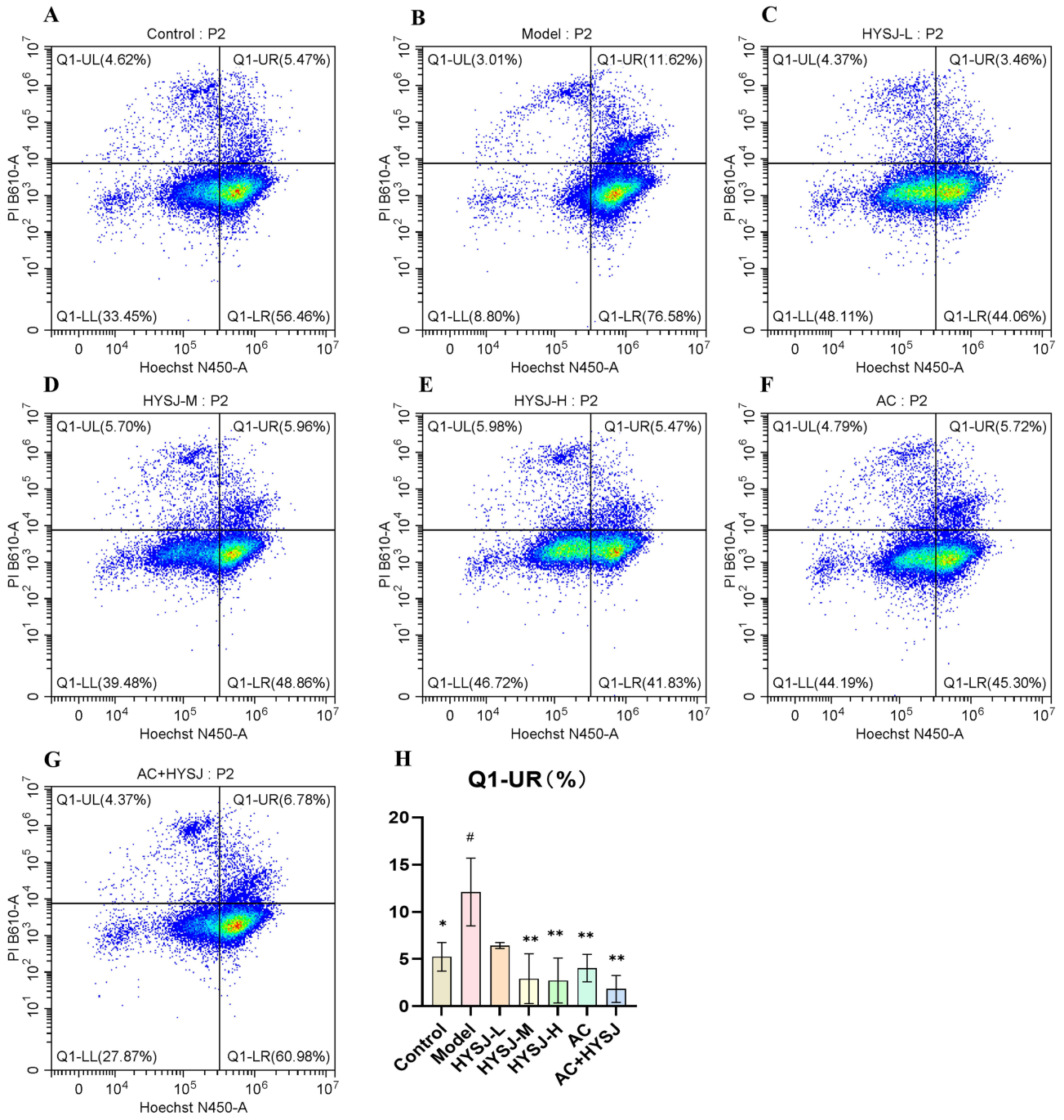

Figure 11 HYSJ inhibits the inflammatory death rate of HLECs. (**A**–**G**) Flow cytometry detection of Hochest/PI double stained HLECs under the indicated intervention conditions. Double positive indicates inflammatory death. (**H**) Analysis of the inflammatory death proportion of HLEC in each group (n=3). $^{\#}P < 0.05$ compared to control group; $^{*}P < 0.05$, $^{**}P < 0.01$ compared to model group.

to the CD44 family of cell-surface glycoproteins and is expressed predominantly in LECs. The protein plays a critical role in lymphangiogenesis and lymphatic function by binding the glycosaminoglycan hyaluronan.[40] LYVE-1 is involved in the clearance of fluids and metabolic waste in the lymphatic system and also is associated with the migration and proliferation of LECs.[41] Diabetic mice exhibited a decrease in LYVE-1 positive lymphatic vessels during corneal wound healing.[42] PROX-1 facilitates the specialization and development of LECs[43] whereas VEGFR3, encoded by the *FLT4* gene, is a tyrosine kinase receptor that is found predominantly on the surface of these cells.[44] VEGF-C plays a crucial role in the development and maintenance of lymphatic vessels by binding to the VEGFR-3 receptor which promotes the

proliferation, migration, and survival of LECs.[45] VEGF-C plays a pivotal role in promoting LEC proliferation and migration through interaction with VEGFR-3.[46] The introduction of the VEGF-C gene in a chronic contact hypersensitivity mouse model alleviated ear swelling and decreased ear weight. Moreover, VEGF-C promoted the clearance of interstitial fluid and inflammatory cells via lymphatic vessels. Conversely, suppression of VEGFR-3 expression markedly impaired the resolution of skin inflammation in this model.[47]

Further analysis of the proteomic profile of wound tissue revealed upregulation of TLR2, Stat1, Myd88, and caspase-1 in the diabetic model group which also was enriched in the inflammatory-related NOD-like receptor pathway. We hypothesize that the mechanism by which HYSJ unguent promotes lymphangiogenesis in DCWs is through inhibition of the NLRP3/caspase-1/GSDMD pathway. To explore this hypothesis, we cultured HLECs in an environment that mimicked the high glucose inflammatory condition of DCWs and analyzed the effects of HYSJ unguent with and without the pyroptosis inhibitor Ac-YVAD-cmk. The latter is a specific inhibitor of caspase-1 that is recognized for its potent anti-inflammatory properties which involves suppression of IL-1β and IL-18 cytokine expression. Ac-YVAD-cmk mitigates pyroptosis across a range of diseases.[48] Both Ac-YVAD-cmk and HYSJ protected HLECs function and promoted the expression of key proteins in the high glucose inflammatory model. HYSJ and Ac-YVAD-cmk inhibited Inflammatory death in HLECs in the high glucose inflammatory environment based on flow cytometry. Therefore, we hypothesize that HYSJ unguent promotes lymphangiogenesis in wounds as illustrated in the graphic abstract. TLR2 recognizes pathogen-associated molecular patterns and damage-associated molecular patterns in HLECs which activates the Myd88-dependent signaling pathway. This stimulation leads to the downstream activation of Stat1 which in turn influences the formation of the inflammasome mediated by caspase-1. Inflammatory cell death is triggered and inflammatory cytokines IL-1β and IL-18 are released. Inhibition of the TLR2/Myd88/caspase-1 axis by HYSJ unguent suppressed inflammatory death in HLECs, protected lymphatic vessels in the wound, and promoted wound healing. This study uniquely integrates proteomic analysis with functional assays, providing comprehensive mechanistic insights that were previously lacking in investigations of HYSJ as a therapeutic for DCW.

DCWs are characterized primarily by persistent inflammation, impaired angiogenesis, and fibroblast dysfunction. Inflammatory cell death plays a significant role in these processes. The high glucose environment in diabetic patients activates the NLRP3 inflammasome and triggers caspase-1-mediated inflammatory cell death. Excessive release of IL-1β and IL-18 during this process causes the local inflammatory response to persist which further deteriorates the wound microenvironment and promotes the formation of chronic non-healing wounds. Astragaloside IV reduces LPS-induced endothelial inflammatory cell death by inhibiting reactive oxygen species production and NLRP3 inflammasome activation. This compound also maintains mitochondrial function by regulating the BCL2/BAX pathway, thereby suppressing the inflammatory response.[49] The NLRP3/caspase-1/GSDMD pathway is activated in the wound tissues of both patients with diabetic foot ulcers and in a DCW murine model.[50] Moreover, knockout of the *CASP-1* and *GSDMD* genes in diabetic mice resulted in a significant acceleration of wound healing. These observations suggest that gasdermin D plays a crucial role as a molecular target in the impaired healing of diabetic foot ulcers. Additionally, polysaccharide from *Bletilla striata* orchid promotes diabetic wound healing by inhibiting the NLRP3 inflammasome and decreasing the secretion of the inflammatory cytokine IL-1β.[51]

HYSJ is an external medication formulated based on prior experience by clinical experts at the Beijing Hospital of Traditional Chinese Medicine. The medication is composed of cinnamon, processed ginger, ginseng, astragalus, ligusticum, angelica, mustard seeds, and baijian which function to warm yang and tonifyi qi, activate blood circulation, and promote tissue regeneration. After application to DCWs, the wound exudate becomes thinner, tissue regeneration and granulation growth are delayed, the wound margins are difficult to contract, and the wound surface appears dull and lacking protection, indicative of a "yang deficiency" state. Over time, the exudate becomes thicker, the color brightens, new granulation tissue forms at the base, epithelial growth occurs at the wound edges, a protective barrier is established, and a marked healing trend is observed which represents a shift to a good state. Throughout the course of our animal experiments, no observable adverse effects related to the application of HYSJU were identified. As a topical formulation, HYSJ Unguent bypasses first-pass hepatic metabolism and renal excretion, thereby minimizing the systemic toxicity commonly associated with systemic drug administration. In comparison to synthetic pharmaceuticals, HYSJ formulated

from renewable plant-based ingredients and produced via low-energy traditional techniques, is likely associated with a relatively lower carbon footprint.[52]

Recent developments in advanced wound dressings, particularly electrospun nanofiber-based biomaterials, have shown great promise in promoting angiogenesis, enhancing cell proliferation, and accelerating the healing of chronic wounds.[53,54] As HYSJ unguent has been used widely in traditional Chinese medicine and is considered relatively safe, future studies should explore the fabrication of HYSJ-loaded nanofiber membranes and hydrogels, assess their physicochemical properties, biocompatibility, and regenerative efficacy, and evaluate their clinical translational potential in chronic wound care. In future studies, we also aim to perform combinatorial and dose–response experiments using isolated or mixed constituents in both in vitro and in vivo models. Such investigations will help clarify the pharmacodynamic contributions of each compound and provide a scientific basis for further optimization and standardization of HYSJ. Inhibition of chronic wound inflammation may be a key strategy in the treatment of DCW with HYSJ unguent as a prospective new candidate drug acting as an anti-inflammatory and wound healing agent.

Conclusion

The principal components of HYSJ unguent include carbohydrates and glycosides, phenylpropanoids, terpenes, amino acids, peptides and derivatives, and fatty acyls. HYSJ unguent promotes lymphangiogenesis in DCWs and inhibits inflammatory death of HLECs under hyperglycemic inflammatory conditions, thereby protecting HLEC. HYSJ has considerable potential as a novel drug to combat chronic wounds in diabetic patients.

Acknowledgments

We are grateful to Guangzhou Genedenovo Biotechnology Co., Ltd for assisting in sequencing and bioinformatics analysis and the LC-MS/MS analysis.

Funding

This study was supported by the National Natural Science Foundation of China (82174388).

Disclosure

The authors report no conflicts of interest in this work.

References

1. Schaper NC, Van Netten JJ, Apelqvist J, et al. Practical guidelines on the prevention and management of diabetes-related foot disease (IWGDF 2023 update). *Diabetes Metab Res Rev*. 2024;40(3):e3657. doi:10.1002/dmrr.3657
2. Yu J, Lee S-H, Kim MK. Recent updates to clinical practice guidelines for diabetes mellitus. *Endocrinol Metab*. 2022;37(1):26–37. doi:10.3803/EnM.2022.105
3. Burgess JL, Wyant WA, Abdo Abujamra B, Kirsner RS, Jozic I. Diabetic wound-healing science. *Medicina*. 2021;57(10):1072. doi:10.3390/medicina57101072
4. Chen N, Deng J, Zhang Z, et al. Oxidative stress-triggered pyroptosis mediates Candida albicans susceptibility in diabetic foot. *Microb Pathogenesis*. 2022;172:105765. doi:10.1016/j.micpath.2022.105765
5. Li J, Chou H, Li L, Li H, Cui Z. Wound healing activity of neferine in experimental diabetic rats through the inhibition of inflammatory cytokines and nrf-2 pathway. *Artif Cells Nanomed Biotechnol*. 2020;48(1):96–106. doi:10.1080/21691401.2019.1699814
6. Chhillar A, Jaiswal A. Hyaluronic acid-based self-healing hydrogels for diabetic wound healing. *Adv Healthcare Mater*. 2025;14(4):2404255. doi:10.1002/adhm.202404255
7. Chen J, Chen D, Chen J, et al. An all-in-one CO gas therapy-based hydrogel dressing with sustained insulin release, anti-oxidative stress, antibacterial, and anti-inflammatory capabilities for infected diabetic wounds. *Acta Biomater*. 2022;146:49–65. doi:10.1016/j.actbio.2022.04.043
8. Zhao X, Pei D, Yang Y, et al. Green tea derivative driven smart hydrogels with desired functions for chronic diabetic wound treatment. *Adv Funct Mater*. 2021;31(18):2009442. doi:10.1002/adfm.202009442
9. Ducoli L, Detmar M. Beyond PROX1: transcriptional, epigenetic, and noncoding RNA regulation of lymphatic identity and function. *Dev Cell*. 2021;56(4):406–426. doi:10.1016/j.devcel.2021.01.018
10. Varricchi G, Granata F, Loffredo S, Genovese A, Marone G. Angiogenesis and lymphangiogenesis in inflammatory skin disorders. *J Am Acad Dermatol*. 2015;73(1):144–153. doi:10.1016/j.jaad.2015.03.041
11. Paavonen K, Puolakkainen P, Jussila L, Jahkola T, Alitalo K. Vascular endothelial growth factor receptor-3 in lymphangiogenesis in wound healing. *Am J Pathol*. 2000;156(5):1499–1504. doi:10.1016/S0002-9440(10)65021-3
12. Scallan JP, Hill MA, Davis MJ. Lymphatic vascular integrity is disrupted in type 2 diabetes due to impaired nitric oxide signalling. *Cardiovascular Res*. 2015;107(1):89–97. doi:10.1093/cvr/cvv117

13. Visuri MT, Honkonen KM, Hartiala P, et al. VEGF-C and VEGF-C156S in the pro-lymphangiogenic growth factor therapy of lymphedema: a large animal study. *Angiogenesis*. 2015;18(3):313–326. doi:10.1007/s10456-015-9469-2
14. Cousin N, Bartel S, Scholl J, et al. Antibody-mediated delivery of VEGF-C promotes long-lasting lymphatic expansion that reduces recurrent inflammation. *Cells*. 2022;12(1):172. doi:10.3390/cells12010172
15. Lin QY, Zhang YL, Bai J, Liu JQ, Li HH. VEGF-C/VEGFR-3 axis protects against pressure-overload induced cardiac dysfunction through regulation of lymphangiogenesis. *Clin Translational Med*. 2021;11(3):e374. doi:10.1002/ctm2.374
16. Yu P, Wu G, Lee HW, Simons M. Endothelial metabolic control of lymphangiogenesis. *Bioessays*. 2018;40(6):1700245. doi:10.1002/bies.201700245
17. Kataru RP, Jung K, Jang C, et al. Critical role of CD11b+ macrophages and VEGF in inflammatory lymphangiogenesis, antigen clearance, and inflammation resolution. *Blood J Am Soc Hematol*. 2009;113(22):5650–5659.
18. Karnam K, Sedmaki K, Sharma P, Venuganti VVK, Kulkarni OP. Selective inhibition of PKR by C16 accelerates diabetic wound healing by inhibiting NALP3 expression in mice. *Inflammation Res*. 2023;72(2):221–236. doi:10.1007/s00011-022-01667-y
19. Lee K-H, Kang T-B. The molecular links between cell death and inflammasome. *Cells*. 2019;8(9):1057. doi:10.3390/cells8091057
20. Miao R, Jiang C, Chang WY, et al. Gasdermin D permeabilization of mitochondrial inner and outer membranes accelerates and enhances pyroptosis. *Immunity*. 2023;56(11):2523–2541.e8. doi:10.1016/j.immuni.2023.10.004
21. Wang Y, Jing L, Lei X, et al. Umbilical cord mesenchymal stem cell-derived apoptotic extracellular vesicles ameliorate cutaneous wound healing in type 2 diabetic mice via macrophage pyroptosis inhibition. *Stem Cell Res Ther*. 2023;14(1):257. doi:10.1186/s13287-023-03490-6
22. Zhou M, Xu X. The effect of huiyang shengji unguent on the healing of yin syndrome wounds in diabetic foot ulcer mice. *Chin J Trad Chin Med*. 2023;38:148–154.
23. Jia X, Xu X, Zhou M. Effects of Huiyang Shengji ointment on oxidative stress in diabetic rats with yin syndrome ulcers. *J Traditional Chin Med*. 2019;60:969–973.
24. Zhou M, Jia X, Xu X. The intervention effect of Huiyang Shengji ointment on human-derived microvascular endothelial cells. *Global Traditional Chin Med*. 2020;13:784–790.
25. Zhou M, Wu L, Tan C, Xu X. Study on the effect of Huiyang Shengji unguent on functional impairment of mouse bone marrow endothelial progenitor cells. *J Beijing University Traditional Chin Med*. 2022;45:41–52.
26. He X, Lin Y, Meng Y, Xue Y, Han X, Li P. Huiyang Shengji Extract improved wound healing by regulating macrophage phenotype transition. *Int J Clin Exp Med*. 2018;11:11690–11705.
27. Liu Q, Zhang J, Han X, et al. Huiyang Shengji decoction promotes wound healing in diabetic mice by activating the EGFR/PI3K/ATK pathway. *ChinMed*. 2021;16(1):1–17. doi:10.1186/s13020-021-00497-0
28. Kim YJ, Chambers AG, Cecchi F, Hembrough T. Targeted data-independent acquisition for mass spectrometric detection of RAS mutations in formalin-fixed, paraffin-embedded tumor biopsies. *J Proteomics*. 2018;189:91–96. doi:10.1016/j.jprot.2018.04.022
29. Wu M, Liu Q, Yu Z, et al. Negative-pressure wound therapy induces lymphangiogenesis in murine diabetic wound healing. *Plastic Reconstructive Surg*. 2023;151(4):779–790. doi:10.1097/PRS.0000000000009997
30. Zhang -J-J, Wang W-L, Zhong J-T, et al. Calycosin limits hepatic fibrogenesis via KLF15 dependent repression of P2X7R in thioacetamide-induced hepatic fibrosis. *J Ethnopharmacol*. 2025;352:120194. doi:10.1016/j.jep.2025.120194
31. Zhang L, Wu Q, Huang Y, Zheng J, Guo S, He L. Formononetin ameliorates airway inflammation by suppressing ESR1/NLRP3/Caspase-1 signaling in asthma. *Biomed Pharmacother*. 2023;168:115799. doi:10.1016/j.biopha.2023.115799
32. Yu T, Lu X, Liang Y, Yang L, Yin Y, Chen H. Ononin alleviates DSS-induced colitis through inhibiting NLRP3 inflammasome via triggering mitophagy. *Immun Inflammation Dis*. 2023;11(2):e776. doi:10.1002/iid3.776
33. Lee HS, Chauhan SK, Okanobo A, Nallasamy N, Dana R. Therapeutic efficacy of topical epigallocatechin gallate in murine dry eye. *Cornea*. 2011;30(12):1465–1472. doi:10.1097/ICO.0b013e31821c9b5a
34. Zhuang T, Lei Y, Chang -J-J, et al. A2AR-mediated lymphangiogenesis via VEGFR2 signaling prevents salt-sensitive hypertension. *Eur Heart J*. 2023;44(29):2730–2742. doi:10.1093/eurheartj/ehad377
35. Renò F, Sabbatini M. Breaking a vicious circle: lymphangiogenesis as a new therapeutic target in wound healing. *Biomedicines*. 2023;11(3):656. doi:10.3390/biomedicines11030656
36. Xie H, Sha S, Lu L, et al. Cerium-containing bioactive glasses promote in vitro lymphangiogenesis. *Pharmaceutics*. 2022;14(2):225. doi:10.3390/pharmaceutics14020225
37. Güç E, Briquez PS, Foretay D, et al. Local induction of lymphangiogenesis with engineered fibrin-binding VEGF-C promotes wound healing by increasing immune cell trafficking and matrix remodeling. *Biomaterials*. 2017;131:160–175. doi:10.1016/j.biomaterials.2017.03.033
38. Onishi T, Nishizuka T, Kurahashi T, et al. Topical bFGF improves secondary lymphedema through lymphangiogenesis in a rat tail model. *Plastic Reconstructive Surg Global Open*. 2014;2(8):e196. doi:10.1097/GOX.0000000000000154
39. Zhu J, Dugas-Ford J, Chang M, et al. Simultaneous in vivo imaging of blood and lymphatic vessel growth in Prox1–GFP/Flk1:: myr–mCherry mice. *FEBS J*. 2015;282(8):1458–1467. doi:10.1111/febs.13234
40. Jackson DG. Biology of the lymphatic marker LYVE-1 and applications in research into lymphatic trafficking and lymphangiogenesis. *Apmis*. 2004;112(7-8):526–538. doi:10.1111/j.1600-0463.2004.apm11207-0811.x
41. Jackson DG. The lymphatics revisited: new perspectives from the hyaluronan receptor LYVE-1. *Trend Cardiovasc Med*. 2003;13(1):1–7. doi:10.1016/S1050-1738(02)00189-5
42. Maruyama K, Asai J, Ii M, Thorne T, Losordo DW, D'Amore PA. Decreased macrophage number and activation lead to reduced lymphatic vessel formation and contribute to impaired diabetic wound healing. *Am J Pathol*. 2007;170(4):1178–1191. doi:10.2353/ajpath.2007.060018
43. Labanaris AP, Polykandriotis E, Horch RE. The effect of vacuum-assisted closure on lymph vessels in chronic wounds. *J Plast Reconstruct Aesthetic Surg*. 2009;62(8):1068–1075. doi:10.1016/j.bjps.2008.01.006
44. Kannan S, Rutkowski JM. VEGFR-3 signaling in macrophages: friend or foe in disease? *Front Immunol*. 2024;15:1349500. doi:10.3389/fimmu.2024.1349500
45. Saaristo A, Tammela T, Fārkkilā A, et al. Vascular endothelial growth factor-C accelerates diabetic wound healing. *Am J Pathol*. 2006;169(3):1080–1087. doi:10.2353/ajpath.2006.051251
46. Huggenberger R, Ullmann S, Proulx ST, Pytowski B, Alitalo K, Detmar M. Stimulation of lymphangiogenesis via VEGFR-3 inhibits chronic skin inflammation. *J Exp Med*. 2010;207(10):2255–2269. doi:10.1084/jem.20100559

47. Hagura A, Asai J, Maruyama K, Takenaka H, Kinoshita S, Katoh N. The VEGF-C/VEGFR3 signaling pathway contributes to resolving chronic skin inflammation by activating lymphatic vessel function. *J Dermatological Sci*. 2014;73(2):135–141. doi:10.1016/j.jdermsci.2013.10.006
48. Liang H, Sun Y, Gao A, et al. Ac-YVAD-cmk improves neurological function by inhibiting caspase-1-mediated inflammatory response in the intracerebral hemorrhage of rats. *Int Immunopharmacol*. 2019;75:105771. doi:10.1016/j.intimp.2019.105771
49. Su Y, Yin X, Huang X, Guo Q, Ma M, Guo L. The BCL2/BAX/ROS pathway is involved in the inhibitory effect of astragaloside IV on pyroptosis in human umbilical vein endothelial cells. *Pharm Biol*. 2022;60(1):1812–1818. doi:10.1080/13880209.2022.2101668
50. Yang S, Feng Y, Chen L, et al. Disulfiram accelerates diabetic foot ulcer healing by blocking NET formation via suppressing the NLRP3/Caspase-1/GSDMD pathway. *Transl Res*. 2023;254:115–127. doi:10.1016/j.trsl.2022.10.008
51. Zhao Y, Wang Q, Yan S, et al. Bletilla striata polysaccharide promotes diabetic wound healing through inhibition of the NLRP3 inflammasome. *Front Pharmacol*. 2021;12:659215. doi:10.3389/fphar.2021.659215
52. Kharissova AB, Kharissova OV, Kharisov BI, Méndez YP. Carbon negative footprint materials: a review. *Nano-Struct Nano-Objects*. 2024;37:101100. doi:10.1016/j.nanoso.2024.101100
53. Augustine R, Hasan A, Patan NK, et al. Titanium nanorods loaded PCL meshes with enhanced blood vessel formation and cell migration for wound dressing applications. *Macromol biosci*. 2019;19(7):1900058. doi:10.1002/mabi.201900058
54. Augustine R, Hasan A, Patan NK, et al. Cerium oxide nanoparticle incorporated electrospun poly (3-hydroxybutyrate-co-3-hydroxyvalerate) membranes for diabetic wound healing applications. *ACS Biomater Sci Eng*. 2019;6(1):58–70. doi:10.1021/acsbiomaterials.8b01352